

SPEED: SCALABLE, PRECISE, AND EFFICIENT CONCEPT ERASURE FOR DIFFUSION MODELS

Ouxiang Li^{1*}, Yuan Wang^{1*}, Xinting Hu^{1†}, Houcheng Jiang¹, Yanbin Hao², Fuli Feng^{1†}

¹University of Science and Technology of China, ²Hefei University of Technology

lioox@mail.ustc.edu.cn, joyhu1412@gmail.com, fulifeng93@gmail.com

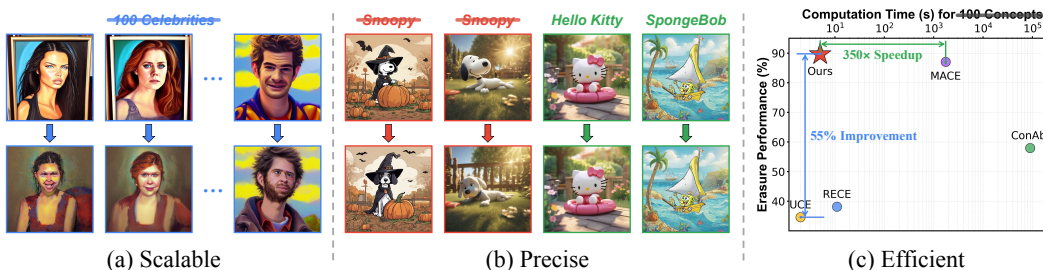


Figure 1: **Three characteristics of our proposed concept erasure method for diffusion models, SPEED.** (a) **Scalable:** SPEED seamlessly scales from single-concept to large-scale multi-concept erasure (e.g., 100 celebrities) without additional design. (b) **Precise:** SPEED precisely removes the target concept (e.g., *Snoopy*) while preserving the semantics for non-target concepts (e.g., *Hello Kitty* and *SpongeBob*). (c) **Efficient:** SPEED immediately erases 100 concepts within 5 seconds, achieving new state-of-the-art (SOTA) performance with a 350× speedup over competitive methods.

ABSTRACT

Erasing concepts from large-scale text-to-image (T2I) diffusion models has become increasingly crucial due to the growing concerns over copyright infringement, privacy violations, and offensive content. In scalable erasure applications, fine-tuning-based methods are time-consuming to precisely erase multiple target concepts, while real-time editing-based methods often degrade the generation quality of non-target concepts due to conflicting optimization objectives. To address this dilemma, we introduce SPEED, a *scalable, precise, and efficient* concept erasure approach that directly edits model parameters. SPEED searches for a null space, a model editing space where parameter updates do not affect non-target concepts, to achieve scalable and precise erasure. To facilitate accurate null space optimization, we incorporate three complementary strategies: Influence-based Prior Filtering (IPF) to selectively retain the most affected non-target concepts, Directed Prior Augmentation (DPA) to enrich the filtered retain set with semantically consistent variations, and Invariant Equality Constraints (IEC) to preserve key invariants during the T2I generation process. Extensive evaluations across multiple concept erasure tasks demonstrate that SPEED consistently outperforms existing methods in non-target preservation while achieving efficient and high-fidelity concept erasure, successfully erasing 100 concepts within only 5 seconds. Our code and models are available at: <https://github.com/Ouxiang-Li/SPEED>.

1 INTRODUCTION

Text-to-image (T2I) diffusion models (Ho et al., 2020; Song et al., 2020a;b; Nichol & Dhariwal, 2021; Rombach et al., 2022; Ho & Salimans, 2022) have facilitated significant breakthroughs in generating highly realistic and contextually consistent images simply from textual descriptions (Dhariwal & Nichol, 2021; Ramesh et al., 2021; Gal et al., 2022; Betker et al., 2023; Ruiz et al., 2023; Podell et al., 2023; Esser et al., 2024; Xu et al., 2025a;b). Alongside these advancements, concerns

*Equal Contributions.

†Corresponding authors.

have also been raised regarding copyright violations (Cui et al., 2023; Shan et al., 2023; Yan et al., 2024), privacy concerns (Carlini et al., 2023; Yang et al., 2023), and offensive content (Schramowski et al., 2023; Yang et al., 2024b; Zhang et al., 2025). To mitigate ethical and legal risks in generation, it is necessary to prevent the model from generating certain concepts, a process termed *concept erasure* (Kumari et al., 2023; Gandikota et al., 2023; Zhang et al., 2024a). However, removing targeted concepts without carefully preserving the semantics of non-target concepts can introduce unintended artifacts, distortions, and degraded image quality (Gandikota et al., 2023; Orgad et al., 2023; Schramowski et al., 2023; Zhang et al., 2024a), compromising the model’s usability. Therefore, beyond ensuring the effective removal of target concepts (*i.e.*, *erasure efficacy*), concept erasure should also maintain the original semantics of non-target concepts (*i.e.*, *prior preservation*).

In this context, recent methods strive to seek a balance between erasure efficacy and prior preservation, broadly categorized into two paradigms: training-based (Kumari et al., 2023; Lyu et al., 2024; Lu et al., 2024a) and editing-based (Gandikota et al., 2024; Gong et al., 2025). The training-based paradigm fine-tunes diffusion models to achieve concept erasure, incorporating an additional regularization into the training objective for prior preservation. In contrast, the editing-based paradigm avoids additional fine-tuning by directly modifying model parameters (*e.g.*, projection weights in cross-attention layers (Rombach et al., 2022)), with such modifications derived from a closed-form objective that jointly accounts for erasure and preservation. This efficiency also facilitates editing-based methods to extend to multi-concept erasure without additional designs seamlessly.

However, as the number of target concepts increases, current editing-based methods (Gandikota et al., 2024; Gong et al., 2025) struggle to balance between erasure efficacy and prior preservation. This can be attributed to the growing conflicts between erasure and preservation objectives, making such trade-offs increasingly difficult. Moreover, these methods rely on weighted least squares optimization, inherently imposing a *non-zero lower bound* on preservation error (see Appx. B.2). In multi-concept settings, this accumulation of preservation errors gradually distorts non-target knowledge, thereby degrading prior preservation. To address the above limitations, we propose a Scalable, Precise, and Efficient Concept Erasure for Diffusion Models (SPEED) (see Fig. 1), an editing-based method with null-space constraints. Specifically, we search for the *null space of prior knowledge*, a model editing space where parameter updates do not affect the feature representations of non-target concepts. By projecting the model parameter updates for concept erasure onto this null space, SPEED can minimize the preservation error to zero without compromising erasure efficacy, thereby enabling scalable and precise concept erasure without affecting non-target concepts.

The main contribution of SPEED lies in defining an effective null space from a set of pre-defined non-target concepts (*i.e.*, *retain set*). We observe that the existing baseline with null-space constraints (Fang et al., 2024) confronts a fundamental dilemma during concept erasure: While a small retain set limits the coverage of prior knowledge, enlarging the retain set makes it increasingly difficult to identify an accurate null space. This dilemma arises because a large retain set drives the corresponding feature matrix toward full rank, necessitating the estimation of its null space to ensure sufficient degrees of freedom for concept erasure. However, such estimation inevitably perturbs the representations of the retain set concepts, leading to semantic degradation and compromised prior preservation, as illustrated in Fig. 2.

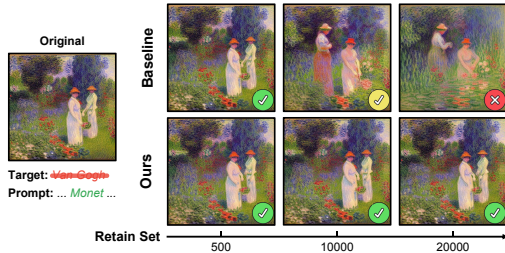


Figure 2: **Semantic degradation with increasing retain set concepts.** The baseline null-space constrained method (Fang et al., 2024) preserves non-target semantics well given a small retain set (✔). However, as the retain set concepts increase, the corresponding matrix approaches higher rank, making the null space estimation increasingly inaccurate (see Eq. 4) with inevitable approximation errors, thereby degrading prior preservation (✔✘).

In this light, we introduce *Prior Knowledge Refinement*, a suite of techniques designed to strategically and selectively refine the retain set so as to mitigate the semantic degradation in searching for the null space. Particularly, we propose *Influence-based Prior Filtering (IPF)*, which first quantifies the influence of concept erasure on each non-target concept and then prunes the retain set by removing minimally affected concepts, preventing the correlation matrix from approaching full rank and thus maintaining an accurate null space. Subsequently, to further enhance prior preservation over the resulting retain set, we propose *Directed Prior Augmentation (DPA)*, which expands the retain

set with directed, semantically consistent perturbations to improve retain set coverage. In addition, we incorporate *Invariant Equality Constraints (IEC)*, which impose equality constraints on invariant representations during generation (e.g., [SOT] token), ensuring that they remain unchanged throughout concept erasure. We evaluate SPEED on three representative concept erasure tasks, i.e., few-concept, multi-concept, and implicit concept erasure, where it consistently exhibits superior prior preservation across all erasure tasks. Our contributions can be summarized as follows:

- We propose SPEED, a scalable, precise, and efficient concept erasure method with null-space constrained model editing, capable of erasing 100 concepts in 5 seconds.
- We introduce Prior Knowledge Refinement to construct an accurate null space over the retain set for effective editing. Leveraging three complementary techniques, IPF, DPA, and IEC, our method balances semantic degradation and retain coverage, enabling precise and scalable concept erasure.
- Our extensive experiments show that SPEED consistently outperforms existing methods in prior preservation across various erasure tasks with minimal computational costs.

2 RELATED WORKS

Concept erasure. Current T2I diffusion models inevitably involve unauthorized and offensive generations due to the noisy training data from web (Schuhmann et al., 2021; 2022). Apart from applying additional filters or safety checkers (Rando et al., 2022; Betker et al., 2023; Rao, 2023), prevailing methods modify diffusion model parameters to erase specific target concepts, mainly categorized into two paradigms. The training-based paradigm fine-tunes model parameters with specific erasure objectives (Kumari et al., 2023; Gandikota et al., 2023; Zhang et al., 2024a;b; Zhao et al., 2024b;a; Huang et al., 2024; Kim et al., 2024; Wu et al., 2025a) and additional regularization. In contrast, the editing-based paradigm edits model parameters using a closed-form solution to facilitate efficiency in concept erasure (Orgad et al., 2023; Gandikota et al., 2024; Gong et al., 2025). These methods can erase numerous concepts within seconds, demonstrating superior efficiency in practice. Beyond parameter modification, non-parametric methods (e.g., external modules and sampling interventions) have also been explored (Schramowski et al., 2023; Wang et al., 2024b; Yoon et al., 2024; Jain et al., 2024; Lee et al., 2025b;a), but they are fragile in open-source settings.

Null-space constraints. The null space of a matrix, a fundamental concept in linear algebra, refers to the set of all vectors that the matrix maps to the zero vector. The null-space constraints are first applied to continual learning by projecting gradients onto the null space of uncentered covariances from previous tasks (Wang et al., 2021). Subsequent studies (Lu et al., 2024b; Wang et al., 2024a; Yang et al., 2024a; Kong et al., 2022; Lin et al., 2022) further explore and extend the application of null space in continual learning. In model editing, AlphaEdit (Fang et al., 2024) restricts model weight updates onto the null space of preserved knowledge, effectively mitigating trade-offs between editing and preservation. Null-space constraints also apply to various tasks, e.g., machine unlearning (Chen et al., 2024), MRI reconstruction (Feng et al., 2023), and image restoration (Wang et al., 2022), offering promise for editing-based concept erasure.

3 PROBLEM FORMULATION

In T2I diffusion models, each concept is encoded by a set of text tokens via CLIP (Radford et al., 2021), which are then aggregated into a single concept embedding $\mathbf{c} \in \mathbb{R}^{d_0}$. For concept erasure, there are two sets of concepts: the erasure set \mathbf{E} and the retain set \mathbf{R} . The erasure set consists of N_E target concepts to be removed, denoted as $\mathbf{E} = \{\mathbf{c}_1^{(i)}\}_{i=1}^{N_E}$. The retain set includes N_R non-target concepts that should be preserved during editing, denoted as $\mathbf{R} = \{\mathbf{c}_0^{(j)}\}_{j=1}^{N_R}$. To enable efficient erasure efficacy for \mathbf{E} and prior preservation for \mathbf{R} , we first formulate a closed-form editing objective in Sec. 3.1, and enhance it with null-space constrained optimization in Sec. 3.2.

3.1 CONCEPT ERASURE IN CLOSED-FORM SOLUTION

To effectively erase each target concept $\mathbf{c}_1^{(i)} \in \mathbf{E}$ (e.g., *Sn00py*), it is specified to be mapped onto an anchor concept $\mathbf{c}_*^{(i)}$ that shares general semantics (e.g., *Dog*), termed as an anchor set

$\mathbf{A} = \{\mathbf{c}_*^{(i)}\}_{i=1}^{N_E}$. For editing-based methods (Orgad et al., 2023; Gandikota et al., 2024; Gong et al., 2025), concept embeddings from the erasure set \mathbf{E} , anchor set \mathbf{A} , and retain set \mathbf{R} are first organized into three structured matrices: $\mathbf{C}_1, \mathbf{C}_* \in \mathbb{R}^{d_0 \times N_E}$ and $\mathbf{C}_0 \in \mathbb{R}^{d_0 \times N_R}$, representing the stacked embeddings of target, anchor, and non-target concepts, respectively. To derive a closed-form solution for concept erasure, existing methods typically optimize a perturbation Δ to model parameters \mathbf{W} , balancing between erasure efficacy and prior preservation. For example, UCE (Gandikota et al., 2024) formulates concept erasure as a weighted least squares problem:

$$\Delta_{\text{UCE}} = \arg \min_{\Delta} \underbrace{\|(\mathbf{W} + \Delta)\mathbf{C}_1 - \mathbf{W}\mathbf{C}_*\|^2}_{e_1} + \underbrace{\|\Delta\mathbf{C}_0\|^2}_{e_0}, \quad (1)$$

where the erasure error e_1 ensures that each target concept is mapped onto its corresponding anchor concept and the preservation error e_0 minimizes the impact on non-target concepts, and $\|\cdot\|^2$ denotes the sum of the squared elements in the matrix (*i.e.*, *Frobenius norm*). This formulation provides a closed-form solution Δ_{UCE} (see Appx. B.1) for parameter updates, achieving computationally efficient optimization. However, as the number of target concepts increases, the accumulated preservation errors e_0 , which admit a provable non-zero bound (see Appx. B.2), across multiple target concepts would amplify the impact on non-target knowledge and degrade prior preservation.

3.2 APPLY NULL-SPACE CONSTRAINTS

To address the limitation of weighted optimization in prior preservation, SPEED incorporates null-space constraints (Wang et al., 2021; Fang et al., 2024) to achieve prior-preserved model editing by forcing $e_0 = 0$. The null space of \mathbf{C}_0 consists of all vectors \mathbf{v} such that $\mathbf{v}\mathbf{C}_0 = \mathbf{0}$. Restricting the parameter update Δ to this space ensures that such updates do not interfere with non-target concepts.

To project Δ onto null space, we apply singular value decomposition (SVD) on $\mathbf{C}_0\mathbf{C}_0^\top \in \mathbb{R}^{d_0 \times d_0}$ ¹ and have $\{\mathbf{U}, \mathbf{\Lambda}, \mathbf{U}^\top\} = \text{SVD}(\mathbf{C}_0\mathbf{C}_0^\top)$, where $\mathbf{U} \in \mathbb{R}^{d_0 \times d_0}$ contains the singular vectors of $\mathbf{C}_0\mathbf{C}_0^\top$, and $\mathbf{\Lambda}$ is a diagonal matrix of its singular values. The singular vectors in \mathbf{U} w.r.t. zero singular values form an orthonormal basis for the null space of \mathbf{C}_0 , which we denote as $\hat{\mathbf{U}}$. Using this basis, we construct the null-space projection matrix $\mathbf{P} = \hat{\mathbf{U}}\hat{\mathbf{U}}^\top$. This process is formulated as:

$$\{\mathbf{U}, \mathbf{\Lambda}, \mathbf{U}^\top\} = \text{SVD}(\mathbf{C}_0\mathbf{C}_0^\top), \quad \hat{\mathbf{U}} = \mathbf{U}[:, \mathbf{\Lambda}_{ii} = 0], \quad \mathbf{P} = \hat{\mathbf{U}}\hat{\mathbf{U}}^\top. \quad (2)$$

The final update applied to model parameters is $\Delta\mathbf{P}$, which projects Δ onto the null space of \mathbf{C}_0 . This ensures that updates do not interfere with non-target concepts, satisfying $\|(\Delta\mathbf{P})\mathbf{C}_0\|^2 = 0$. To solve for the updates, we minimize the following objective:

$$\Delta_{\text{Null}} = \arg \min_{\Delta} \underbrace{\|(\mathbf{W} + \Delta\mathbf{P})\mathbf{C}_1 - \mathbf{W}\mathbf{C}_*\|^2}_{e_1} + \underbrace{\|(\Delta\mathbf{P})\mathbf{C}_0\|^2}_{e_0=0} + \underbrace{\|\Delta\mathbf{P}\|^2}_{\text{regularization}}, \quad (3)$$

where $\|\Delta\mathbf{P}\|^2$ is a regularization term to ensure convergence. The preservation term $\|(\Delta\mathbf{P})\mathbf{C}_0\|^2$ is omitted, as it is guaranteed to be zero by the null-space constraint ($e_0 = 0$). This objective allows the model parameters to be updated such that target concepts are effectively erased while representations of non-target concepts remain unaffected, thereby achieving prior-preserved concept erasure.

4 PRIOR KNOWLEDGE REFINEMENT

However, as more diverse non-target concepts are included in the retain set, the rank of the correlation matrix $\mathbf{C}_0\mathbf{C}_0^\top$ gradually increases². The null space, defined as the orthogonal complement of this span, correspondingly shrinks in dimension:

$$\dim(\text{Null}(\mathbf{C}_0\mathbf{C}_0^\top)) = d_0 - \text{rank}(\mathbf{C}_0\mathbf{C}_0^\top). \quad (4)$$

Here, the null space dimension characterizes the degrees of freedom available for editing without affecting the non-target concepts. However, as this dimension shrinks, to ensure sufficient degrees of

¹ $\mathbf{C}_0\mathbf{C}_0^\top$ and \mathbf{C}_0 share the same null space. We operate on $\mathbf{C}_0\mathbf{C}_0^\top \in \mathbb{R}^{d_0 \times d_0}$ since it has fixed row dimension while $\mathbf{C}_0 \in \mathbb{R}^{d_0 \times N_R}$ may have high dimensionality depending on concept number N_R .

²We assume that the concepts are not exactly linearly dependent in the representation space, which is generally satisfied in practice due to the semantic diversity and high dimensionality of the embedding space.

freedom for concept erasure, we are compelled to include additional singular vectors w.r.t. non-zero singular values in $\tilde{\mathbf{U}}$ following (Fang et al., 2024), which leads to an approximate null space and induces semantic degradation (see Fig. 2). To improve, we propose **Prior Knowledge Refinement**, a structured strategy for refining the retain set to enable accurate null-space construction, with three complementary techniques: (1) Influence-Based Prior Filtering (Sec. 4.1) to discard weakly affected non-target concepts to form a viable null space; (2) Directed Prior Augmentation (Sec. 4.2) to expand the retain set with targeted and semantically consistent variations; and (3) Invariant Equality Constraints (Sec. 4.3) to enforce equality constraints to preserve critical invariants during generation.

4.1 INFLUENCE-BASED PRIOR FILTERING (IPF)

Given a predefined retain set, existing editing-based methods (Gandikota et al., 2024; Gong et al., 2025) treat all non-target concepts equally when enforcing prior preservation. However, an overlooked fact is that parameter updates inherently induce output changes over non-target concepts, and these changes vary across different non-target concepts. This suggests that not all non-target concepts contribute equally to preserving prior knowledge, and weakly influenced concepts offer little benefit but introduce additional ranks that narrow the null space.

To this end, we propose an explicit and model-consistent metric (*i.e.*, **prior shift**) to quantify how much a certain non-target concept is affected by concept erasure. Specifically, we isolate the effect of erasure by solving for a closed-form update Δ_{erase} that minimizes only the erasure error e_1 while discarding the preservation term e_0 from Eq. 1:

$$\Delta_{\text{erase}} = \arg \min_{\Delta} \underbrace{\|(\mathbf{W} + \Delta)\mathbf{C}_1 - \mathbf{W}\mathbf{C}_*\|^2}_{e_1} + \underbrace{\|\Delta\|^2}_{\text{regularization}} = \mathbf{W}(\mathbf{C}_*\mathbf{C}_1^\top - \mathbf{C}_1\mathbf{C}_1^\top)(\mathbf{I} + \mathbf{C}_1\mathbf{C}_1) \mathbf{W}^{-1}, \quad (5)$$

where $\|\Delta\|^2$ is introduced for convergence. For each non-target concept embedding \mathbf{c}_0 , we define its prior shift as $\|\Delta_{\text{erase}}\mathbf{c}_0\|^2$. This value offers a faithful reflection of how parameter updates perturb a non-target concept in the feature space with closed-form computation, and can naturally generalize to assessing multi-concept erasure effects. Based on this, we filter the original retain set \mathbf{R} to focus only on highly influenced concepts:

$$\mathbf{R}_f : \mathbf{R} \mapsto \{\mathbf{c}_0 \in \mathbf{R} \mid \|\Delta_{\text{erase}}\mathbf{c}_0\|^2 > \mu\}, \quad (6)$$

where the mean value $\mu = \mathbb{E}_{\mathbf{c}_0 \sim \mathbf{R}} [\|\Delta_{\text{erase}}\mathbf{c}_0\|^2]$ serves as a filtering threshold.

4.2 DIRECTED PRIOR AUGMENTATION (DPA)

To further enhance the prior preservation with broader retain coverage, an intuitive strategy is to augment the retain set by perturbing non-target embedding \mathbf{c}_0 with random noise (Lyu et al., 2024). However, this strategy would introduce meaningless embeddings that fail to generate semantically coherent images (*e.g.*, noise image), resulting in excessive preservation with increasing ranks. To search for more semantically consistent concepts, we introduce directed noise by projecting the random noise ϵ onto the direction in which the model parameters \mathbf{W} exhibit minimal variation. This operation ensures the perturbed embeddings express closer semantics to the original concept after being mapped by \mathbf{W} (see Fig. 3). Specifically, we first derive a projection matrix \mathbf{P}_{\min} :

$$\{\mathbf{U}_{\mathbf{W}}, \Lambda_{\mathbf{W}}, \mathbf{U}_{\mathbf{W}}^\top\} = \text{SVD}(\mathbf{W}), \quad \mathbf{P}_{\min} = \mathbf{U}_{\min} \mathbf{U}_{\min}^\top, \quad (7)$$

where $\mathbf{U}_{\min} = \mathbf{U}_{\mathbf{W}}[:, -r :]$ denotes the singular vectors w.r.t. the smallest r singular vectors³, which represent the r least-changing directions of \mathbf{W} and constrain the rank of the augmented embeddings

³Empirically, the model parameter matrix \mathbf{W} is usually full rank, thus its all singular values are non-zero.

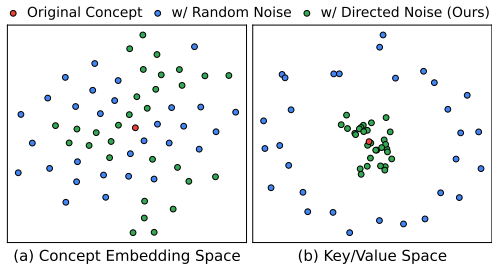


Figure 3: **t-SNE distribution of perturbing the original concept** with *random noise* and *directed noise*. (a) Similar to random noise, our method can span a broad concept embedding space. (b) Our directed noise preserves semantic similarity to the original concept with closer distances in the space mapped by \mathbf{W} .

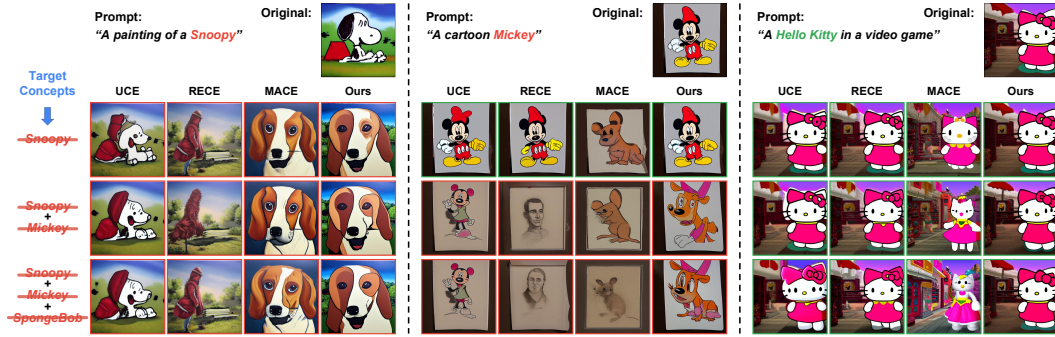


Figure 4: **Qualitative comparison of the few-concept erasure in erasing instances.** The erased and preserved generations are highlighted with red and green boxes, respectively. Our method exhibits consistent prior preservation with less semantic degradation for non-target concepts. For example, the middle column better retains details such as *Mickey*’s hat and button count, and the right column demonstrates more consistent *Hello Kitty* generations along with three concepts erased.

to a maximum of r . Then the directed noise $\epsilon \cdot \mathbf{P}_{\min}$ is used to perturb the original embedding via:

$$\mathbf{c}'_0 = \mathbf{c}_0 + \epsilon \cdot \mathbf{P}_{\min}, \quad \epsilon \sim \mathcal{N}(\mathbf{0}, \mathbf{I}). \quad (8)$$

Given a retain set \mathbf{R} , the augmentation process can be formulated as follows:

$$\mathbf{R}^{\text{aug}} : \mathbf{R} \mapsto \bigcup_{\mathbf{c}_0 \in \mathbf{R}} \{ \mathbf{c}_0 + \epsilon_k \cdot \mathbf{P}_{\min} \mid k = 1, \dots, N_A \}, \quad (9)$$

where N_A denotes the augmentation times and $\mathbf{c}_0 + \epsilon_k \cdot \mathbf{P}_{\min}$ represents the k -th augmented embedding given $\mathbf{c}_0 \in \mathbf{R}$ using Eq. 8. In implementation, we first apply IPF to the original retain set \mathbf{R} to obtain \mathbf{R}_f , and then apply DPA followed by IPF to \mathbf{R}_f to produce $(\mathbf{R}_f)_f^{\text{aug}}$ as augmented concepts. Finally, we combine them to serve as the final refined retain set $\mathbf{R}_{\text{refine}} = \mathbf{R}_f \cup (\mathbf{R}_f)_f^{\text{aug}}$.

4.3 INVARIANT EQUALITY CONSTRAINTS (IEC)

In parallel, we identify certain invariants during the T2I generation process, *i.e.*, intermediate variables that remain unchanged under different sampling prompts. One such invariant is the CLIP-encoded [SOT] token. Since the encoding process is masked by causal attention and all prompts are prefixed with the fixed [SOT] token during tokenization, its embedding consistently remains unchanged during T2I process. Another invariant is the null-text embedding, as it corresponds to the unconditional generation under the classifier-free guidance (Ho & Salimans, 2022), which also remains unchanged despite prompt variations. Given the invariance of these embeddings, we consider additional preservation measures to ensure their outputs remain unchanged during concept erasure. Specifically, we introduce explicit equality constraints over invariants based on Eq. 3:

$$\min_{\Delta} \underbrace{\|(\mathbf{W} + \Delta\mathbf{P})\mathbf{C}_1 - \mathbf{W}\mathbf{C}_*\|^2}_{e_1} + \underbrace{\|\Delta\mathbf{P}\|^2}_{\text{regularization}}, \quad \text{s.t.} \underbrace{(\Delta\mathbf{P})\mathbf{C}_2 = \mathbf{0}}_{\text{equality constraints}} \quad (10)$$

where \mathbf{C}_2 stacks the invariant embeddings of [SOT] and null-text. Using the projection matrix \mathbf{P} constructed from $\mathbf{R}_{\text{refine}}$, we can derive the closed-form solution of Eq. 10 using Lagrange Multipliers from Appx. B.3:

$$(\Delta\mathbf{P})_{\text{Ours}} = \mathbf{W} (\mathbf{C}_* \mathbf{C}_1^\top - \mathbf{C}_1 \mathbf{C}_1^\top) \mathbf{P} \mathbf{Q} \mathbf{M}, \quad (11)$$

where

$$\mathbf{M} = (\mathbf{C}_1 \mathbf{C}_1^\top \mathbf{P} + \mathbf{I})^{-1}, \quad \mathbf{Q} = \mathbf{I} - \mathbf{M} \mathbf{C}_2 (\mathbf{C}_2^\top \mathbf{P} \mathbf{M} \mathbf{C}_2)^{-1} \mathbf{C}_2^\top \mathbf{P}. \quad (12)$$

This closed-form solution enforces the equality constraints by projecting the parameter update onto the subspace orthogonal to the invariant embeddings. Since image generation inevitably depends on these invariant embeddings, such constraints inherently preserve prior knowledge.

Table 1: **Quantitative comparison of the few-concept erasure** on instances (*left*) and artistic styles (*right*), where target concepts are highlighted in pink. Arrows indicate the preferred direction for each metric, and the best results are highlighted in **bold**. Our method consistently improves prior preservation on non-target and general concepts from MS-COCO while achieving effective concept erasure. Although our CS is not always the lowest for target concepts, Appx. D.1 shows our method is sufficient for erasure, and lower CS may further compromise prior preservation.

Concept	Snoopy	Mickey	Spongebob	Pikachu	Hello Kitty	MS-COCO	
	CS	CS	CS	CS	CS	CS	FID
SD v1.4	28.51	26.62	27.30	27.44	27.77	26.53	-
Erase <i>Snoopy</i>							
	CS ↓	FID ↓	FID ↓	FID ↓	FID ↓	CS ↑	FID ↓
ConAbl	25.44	37.08	38.92	26.14	36.52	26.40	21.20
MACE	20.90	105.97	102.77	65.71	75.42	26.09	42.62
RECE	18.38	26.63	34.42	21.99	32.35	26.39	25.61
UCE	23.19	24.87	29.86	19.06	27.86	26.46	22.18
Ours	23.50	23.41	24.64	16.81	21.74	26.48	19.95
Erase <i>Snoopy</i> and <i>Mickey</i>							
	CS ↓	CS ↓	FID ↓	FID ↓	FID ↓	CS ↑	FID ↓
ConAbl	25.26	26.58	45.08	35.57	41.48	26.42	24.34
MACE	20.53	20.63	112.01	91.72	106.88	25.50	55.15
RECE	18.57	19.14	35.85	26.05	40.77	26.31	30.30
UCE	23.60	24.79	30.58	23.51	31.76	26.38	26.06
Ours	23.58	23.62	29.67	22.51	28.23	26.47	23.66
Erase <i>Snoopy</i> and <i>Mickey</i> and <i>Spongebob</i>							
	CS ↓	CS ↓	CS ↓	FID ↓	FID ↓	CS ↑	FID ↓
ConAbl	24.92	26.46	25.12	46.47	48.24	26.37	26.71
MACE	19.86	19.35	20.12	110.12	128.56	23.39	66.39
RECE	18.17	18.87	16.23	40.52	52.06	26.32	32.51
UCE	23.29	24.63	19.08	29.20	38.15	26.30	28.71
Ours	23.69	23.93	21.39	21.40	26.22	26.51	24.99

Concept	Van Gogh	Picasso	Monet	Paul Gauguin	Caravaggio	MS-COCO	
	CS	CS	CS	CS	CS	CS	FID
SD v1.4	28.75	27.98	28.91	29.80	26.27	26.53	-
Erase <i>Van Gogh</i>							
	CS ↓	FID ↓	FID ↓	FID ↓	FID ↓	CS ↑	FID ↓
ConAbl	28.16	77.01	63.80	63.20	79.25	26.46	18.36
MACE	26.66	69.92	60.88	56.18	69.04	26.50	23.15
RECE	26.39	60.57	61.09	47.07	72.85	26.52	23.54
UCE	28.10	43.02	40.49	32.62	61.72	26.54	19.63
Ours	26.29	35.86	16.85	24.94	39.75	26.55	20.36
Erase <i>Picasso</i>							
	FID ↓	CS ↓	FID ↓	FID ↓	FID ↓	CS ↑	FID ↓
ConAbl	60.44	26.97	36.23	65.23	79.12	26.43	20.02
MACE	59.58	26.48	37.02	46.35	66.20	26.47	22.86
RECE	51.09	26.66	25.39	46.08	75.61	26.48	23.03
UCE	37.58	26.99	16.72	32.48	59.27	26.50	20.33
Ours	19.18	26.22	19.87	24.73	43.63	26.51	19.98
Erase <i>Monet</i>							
	FID ↓	FID ↓	CS ↓	FID ↓	FID ↓	CS ↑	FID ↓
ConAbl	68.77	64.25	27.05	57.33	71.88	26.45	21.03
MACE	61.50	48.41	25.98	49.66	65.87	26.47	22.76
RECE	56.26	45.97	25.87	46.38	64.19	26.49	24.94
UCE	42.25	38.73	27.12	33.00	56.49	26.51	21.58
Ours	28.78	41.21	25.06	27.85	55.20	26.48	20.87

5 EXPERIMENTS

In this section, we conduct extensive experiments on three representative erasure tasks, including few-concept erasure, multi-concept erasure, and implicit concept erasure (Appx. D.4), validating our superior prior preservation. The compared baselines include ConAbl (Kumari et al., 2023), MACE (Lu et al., 2024a), RECE (Gong et al., 2025), and UCE (Gandikota et al., 2024), which have achieved SOTA performance across various concept erasure tasks. In implementation, we conduct all experiments on SDv1.4 (Stability AI, 2022) and generate each image using DPM-solver sampler (Lu et al., 2022) over 20 sampling steps with classifier-free guidance (Ho & Salimans, 2022) of 7.5. More implementation details and compared baselines can be found in Appx. C and Appx. D.3.

5.1 ON FEW-CONCEPT ERASURE

Evaluation setup. We evaluate few-concept erasure on instance erasure and artistic style erasure following (Lyu et al., 2024), using 80 instance templates and 30 artistic style templates with 10 images per template per concept. We use two metrics for evaluation: CLIP Score (CS) (Radford et al., 2021) for the text-image similarity and Fréchet Inception Distance (FID) (Heusel et al., 2017) for the distributional distance before and after erasure. Following (Lyu et al., 2024), we select non-target concepts with similar semantics to the target concept for comparison and report CS for targets and FID for non-targets in the main paper. Complete comparisons are presented in Appx. D.2. We further compare the generations on MS-COCO captions (Lin et al., 2014), where we generate images with the first 1,000 captions, and report CS and FID to measure general knowledge preservation.

Analysis and discussion. Table 1 compares the results of erasing various instance concepts and artistic styles. Our method consistently achieves the lowest FIDs across all non-target concepts, demonstrating superior prior preservation with minimal alteration to the original content. Moreover, we emphasize that our erasure is sufficiently effective, even without achieving the lowest CS, as shown in Figs. 4 and 7. On this basis, lower CS values typically indicate “over-erasure” of the target concept, since further reductions in CS after successful erasure usually come at the cost of prior preservation, as detailed in Appx. D.1. Notably, with the number of target concepts increasing from 1 to 3, our FID in *Pikachu* rises from 16.81 to 21.40 (4.59 ↑), while UCE increases from 19.06 to 29.20 (10.14 ↑). A similar pattern is observed in *Hello Kitty* (Our 4.48 ↑ v.s. UCE’s 10.29 ↑), showing our superiority of prior preservation in erasing increasing target concepts.

Table 2: **Quantitative comparison of the multi-concept erasure** in erasing 10, 50, and 100 celebrities. The best results are highlighted in **bold**. Our method can effectively erase up to 100 celebrities simultaneously, achieving low Acc_e (%) and high Acc_r (%) that preserve non-target celebrities with minimal appearance changes. This yields the best overall erasure performance H_o and competitive runtime (s), successfully erasing 100 concepts in just 5 seconds.

	Erase 10 Celebrities				MS-COCO		Erase 50 Celebrities				MS-COCO		Erase 100 Celebrities				MS-COCO	
	$Acc_e \downarrow$	$Acc_r \uparrow$	$H_o \uparrow$	Time \downarrow	CS \uparrow	FID \downarrow	$Acc_e \downarrow$	$Acc_r \uparrow$	$H_o \uparrow$	Time \downarrow	CS \uparrow	FID \downarrow	$Acc_e \downarrow$	$Acc_r \uparrow$	$H_o \uparrow$	Time \downarrow	CS \uparrow	FID \downarrow
SD v1.4	91.99	89.66	14.70	-	26.53	-	93.08	89.66	12.85	-	26.53	-	90.18	89.66	17.70	-	26.53	-
ConAbl	60.76	77.89	52.19	900	25.60	42.12	64.00	75.44	48.74	4,500	14.30	255.36	42.86	58.82	57.97	9,000	14.93	235.27
UCE	0.20	71.19	83.10	1.5	24.07	83.81	0.00	31.94	48.41	1.8	13.45	209.93	0.00	20.92	34.60	2.1	13.49	185.46
RECE	0.34	67.43	80.44	2.5	16.75	170.65	1.03	19.77	32.95	6.3	13.49	213.39	2.43	23.71	38.16	11.0	12.09	177.57
MACE	1.62	87.73	92.75	207	26.36	37.25	3.41	84.31	90.03	936	25.45	45.31	4.80	80.20	87.06	1736	24.80	50.41
Ours	1.81	89.09	93.42	3.8	26.47	30.02	3.46	88.48	92.34	4.2	26.46	39.23	5.87	85.54	89.63	5.0	26.22	44.97

5.2 ON MULTI-CONCEPT ERASURE

Evaluation setup. Another more realistic erasure scenario is multi-concept erasure, where massive concepts are required to be erased at once. We follow the experiment setup in Lu et al. (2024a) for erasing multiple celebrities, where we experiment with erasing 10, 50, and 100 celebrities and collect another 100 celebrities as non-target concepts. Specifically, we prepare 5 prompt templates for each celebrity concept. For non-target concepts, we generate 1 image per template for each of the 100 concepts, totaling 500 images. For target concepts, we adjust the per-concept quantity to maintain a total of 500 images (e.g., erasing 10 celebrities involves generating 10 images with 5 templates per concept). In evaluation, we adopt GIPHY Celebrity Detector (GCD) (Hasty et al., 2019) and measure the top-1 GCD accuracy, indicated by Acc_e for erased target concepts and Acc_r for retained non-target concepts. Meanwhile, the harmonic mean $H_o = \frac{2}{(1-Acc_e)^{-1} + (Acc_r)^{-1}}$ is adopted to assess the overall erasure performance. Additionally, we report the results on MS-COCO to demonstrate the prior preservation of general concepts.

Analysis and discussion. Table 2 showcases a notable improvement of our method on multi-concept erasure, particularly in prior preservation with the highest Acc_r . In comparison with the SOTA method, MACE (Lu et al., 2024a), our method achieves superior prior preservation with better Acc_r , while maintaining comparable erasure efficacy, as reflected in similar Acc_e , resulting in the best overall erasure performance indicated by the highest H_o . Meanwhile, our method attains the lowest FID across all methods on MS-COCO. The other methods, UCE (Gandikota et al., 2024) and RECE (Gong et al., 2025), although achieving considerable balance in few-concept erasure, fail to maintain this balance as the number of target concepts increases as shown in Fig. 5, with catastrophic prior damage evidenced by MS-COCO as well. Notably, our method can erase up to 100 celebrities in 5 seconds, whereas MACE requires around 30 minutes ($\times 350$ time). In real-world scenarios, this efficiency underscores our potential for the instant erasure of massive concepts.

5.3 FURTHER ANALYSIS

More applications on other T2I models. To validate the transferability of our method across versatile applications, we conduct further experiments on various T2I models with different weights and architectures, including: (1) Composite concept erasure on DreamShaper (Lykon, 2023) and RealisticVision (SG161222, 2023) from Fig 6 (a): Our method can precisely erase the target concept(s) while preserving other non-target elements within the prompt, such as the *Van Gogh*-style background (2nd column) and the *Snoopy* character (3rd column). (2) Knowledge editing on SDXL (Podell et al., 2023) from Fig 6 (b): The arbitrary nature of anchor concepts allows us to edit the pre-trained model knowledge. Herein, our method effectively edits the model knowledge while

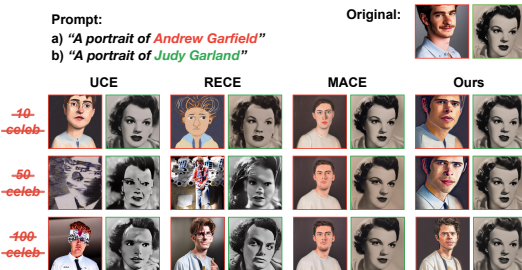


Figure 5: **Quantitative comparison of the multi-concept erasure** in erasing celebrities (*celeb*). The erased and preserved generations are marked with **red** and **green** boxes. Our method precisely erases 100 celebrities while preserving generations of other non-target concepts.

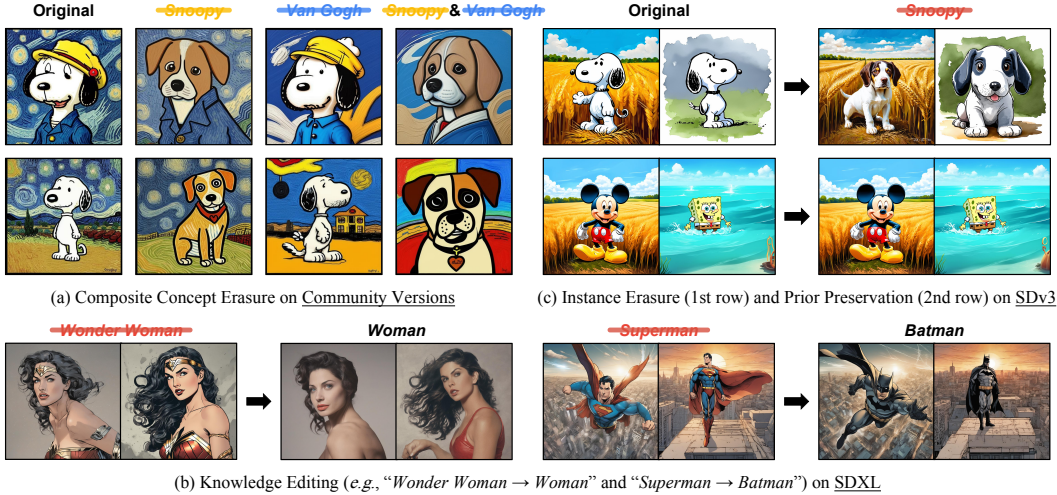


Figure 6: **More applications across various T2I diffusion models.** (a) We conduct composite concept erasure for “Snoopy + Van Gogh” on DreamShaper (Lykon, 2023) (1st row) and RealisticVision (SG161222, 2023) (2nd row). (b) Our method also enables model knowledge editing by specifying the anchor concept on SDXL (Podell et al., 2023). (c) Our method can seamlessly transfer to novel DiT-based T2I models, e.g., SDv3 (Esser et al., 2024).

maintaining the overall layout and semantics of the generated images. (3) Instance erasure on SDv3 (Esser et al., 2024) from Fig 6 (c): To accommodate the diffusion transformer (DiT) (Peebles & Xie, 2023) architecture in T2I models, we adapt our method to a DiT-based model, demonstrating a well-balanced trade-off between erasure (1st row) and preservation (2nd row) as well.

Component ablation. From Table 3, we compare the individual impact of our components on prior preservation and draw the following conclusions: (1) Impact of IEC (Ablation 1 v.s. 2): IEC reduces the non-target FID and the MS-COCO FID, demonstrating its effectiveness by preserving invariant embeddings with equality constraints. (2) Impact of IPF (Ablation 2 v.s. 3): Incorporating IPF results in a significant improvement in both FIDs, underscoring its critical role in filtering out less-influenced concepts in the retain set to mitigate semantic degradation. (3) Impact of DPA (Ablation 4 v.s. Ours): DPA improves RPA with directed noise and leads to a substantial improvement in non-target and MS-COCO FIDs, highlighting its advantage by introducing semantically similar concepts into the refined retain set. To conclude, the proposed three components (*i.e.*, IEC, IPF, and DPA) improve the prior preservation from different perspectives and contribute to our method with the best prior preservation under null space constraints. More ablations are presented in Appx. D.5.

6 CONCLUSION

This paper introduced SPEED, a scalable, precise, and efficient concept erasure method for T2I diffusion models. It formulates concept erasure as a null-space constrained optimization problem, facilitating effective prior preservation along with precise erasure efficacy. Critically, SPEED overcomes the inefficacy of editing-based methods in multi-concept erasure while circumventing the prohibitive computational costs associated with training-based approaches. With our proposed Prior Knowledge Refinement involving three complementary techniques, SPEED not only ensures superior prior preservation but also achieves a 350× acceleration in multi-concept erasure, establishing itself as a scalable and practical solution for real-world applications.

Table 3: **Ablation study** on proposed components in erasing *Van Gogh*, with the non-target FID averaged over the other four artistic styles from Table 1. Ablation 1 corresponds to the original objective from (Fang et al., 2024) in Eq. 3. The ablated components include: IEC (Invariant Equality Constraints), IPF (Influence-based Prior Filtering), RPA (Random Prior Augmentation), and DPA (Directed Prior Augmentation).

Ablation	Components				Target CS ↓	Non-Target FID ↓	MS-COCO	
	IEC	IPF	RPA	DPA			CS ↑	FID ↓
1	×	×	×	×	27.20	50.43	26.42	26.33
2	✓	×	×	×	27.20	48.17	26.44	24.95
3	✓	✓	×	×	26.68	38.02	26.54	20.57
4	✓	✓	✓	×	26.30	32.62	26.52	20.99
Ours	✓	✓	×	✓	26.29	29.35	26.55	20.36
SD v1.4	-	-	-	-	28.75	-	26.53	-

ETHICS STATEMENT

This work introduces a method for concept erasure in text-to-image diffusion models to address ethical concerns such as copyright infringement, privacy violations, and the generation of offensive content. By precisely removing specific target concepts while preserving the quality and semantics of non-target outputs, the proposed approach enhances the safety, reliability, and controllability of generative models. The method operates through parameter-space editing without requiring access to private data or involving human subjects, ensuring ethical integrity throughout the research process and promoting responsible deployment of generative AI technologies.

REFERENCES

- Josh Achiam, Steven Adler, Sandhini Agarwal, Lama Ahmad, Ilge Akkaya, Florencia Leoni Aleman, Diogo Almeida, Janko Altenschmidt, Sam Altman, Shyamal Anadkat, et al. Gpt-4 technical report. *arXiv preprint arXiv:2303.08774*, 2023.
- Amazon. Amazon Mechanical Turk: Crowdsourcing Marketplace. <https://www.mturk.com/>.
- P Bedapudi. Nudenet: Neural nets for nudity classification, detection and selective censoring, 2019.
- James Betker, Gabriel Goh, Li Jing, Tim Brooks, Jianfeng Wang, Linjie Li, Long Ouyang, Juntang Zhuang, Joyce Lee, Yufei Guo, et al. Improving image generation with better captions. *Computer Science*. <https://cdn.openai.com/papers/dall-e-3.pdf>, 2(3):8, 2023.
- Nicolas Carlini, Jamie Hayes, Milad Nasr, Matthew Jagielski, Vikash Sehwal, Florian Tramèr, Borja Balle, Daphne Ippolito, and Eric Wallace. Extracting training data from diffusion models. In *32nd USENIX Security Symposium (USENIX Security 23)*, pp. 5253–5270, 2023.
- Huiqiang Chen, Tianqing Zhu, Xin Yu, and Wanlei Zhou. Machine unlearning via null space calibration. *arXiv preprint arXiv:2404.13588*, 2024.
- Yingqian Cui, Jie Ren, Han Xu, Pengfei He, Hui Liu, Lichao Sun, Yue Xing, and Jiliang Tang. Diffusionshield: A watermark for copyright protection against generative diffusion models. *arXiv preprint arXiv:2306.04642*, 2023.
- Prafulla Dhariwal and Alexander Nichol. Diffusion models beat gans on image synthesis. *Advances in neural information processing systems*, 34:8780–8794, 2021.
- Patrick Esser, Robin Rombach, and Bjorn Ommer. Taming transformers for high-resolution image synthesis. In *Proceedings of the IEEE/CVF conference on computer vision and pattern recognition*, pp. 12873–12883, 2021.
- Patrick Esser, Sumith Kulal, Andreas Blattmann, Rahim Entezari, Jonas Müller, Harry Saini, Yam Levi, Dominik Lorenz, Axel Sauer, Frederic Boesel, et al. Scaling rectified flow transformers for high-resolution image synthesis. In *Forty-first International Conference on Machine Learning*, 2024.
- Junfeng Fang, Houcheng Jiang, Kun Wang, Yunshan Ma, Xiang Wang, Xiangnan He, and Tat-seng Chua. Alphaedit: Null-space constrained knowledge editing for language models. *arXiv preprint arXiv:2410.02355*, 2024.
- Chun-Mei Feng, Bangjun Li, Xinxing Xu, Yong Liu, Huazhu Fu, and Wangmeng Zuo. Learning federated visual prompt in null space for mri reconstruction. In *Proceedings of the IEEE/CVF Conference on Computer Vision and Pattern Recognition*, pp. 8064–8073, 2023.
- Rinon Gal, Yuval Alaluf, Yuval Atzmon, Or Patashnik, Amit H Bermano, Gal Chechik, and Daniel Cohen-Or. An image is worth one word: Personalizing text-to-image generation using textual inversion. *arXiv preprint arXiv:2208.01618*, 2022.
- Rohit Gandikota, Joanna Materzynska, Jaden Fiotto-Kaufman, and David Bau. Erasing concepts from diffusion models. In *Proceedings of the IEEE/CVF International Conference on Computer Vision*, pp. 2426–2436, 2023.

- Rohit Gandikota, Hadas Orgad, Yonatan Belinkov, Joanna Materzyńska, and David Bau. Unified concept editing in diffusion models. In *Proceedings of the IEEE/CVF Winter Conference on Applications of Computer Vision*, pp. 5111–5120, 2024.
- Chao Gong, Kai Chen, Zhipeng Wei, Jingjing Chen, and Yu-Gang Jiang. Reliable and efficient concept erasure of text-to-image diffusion models. In *European Conference on Computer Vision*, pp. 73–88. Springer, 2025.
- Nick Hasty, Ihor Kroosh, Dmitry Voitek, and Dmytro Korduban. Giphy celebrity detector. <https://github.com/Giphy/celeb-detection-oss>, 2019.
- Amir Hertz, Ron Mokady, Jay Tenenbaum, Kfir Aberman, Yael Pritch, and Daniel Cohen-Or. Prompt-to-prompt image editing with cross attention control. *arXiv preprint arXiv:2208.01626*, 2022.
- Martin Heusel, Hubert Ramsauer, Thomas Unterthiner, Bernhard Nessler, and Sepp Hochreiter. Gans trained by a two time-scale update rule converge to a local nash equilibrium. *Advances in neural information processing systems*, 30, 2017.
- Jonathan Ho and Tim Salimans. Classifier-free diffusion guidance. *arXiv preprint arXiv:2207.12598*, 2022.
- Jonathan Ho, Ajay Jain, and Pieter Abbeel. Denoising diffusion probabilistic models. *Advances in neural information processing systems*, 33:6840–6851, 2020.
- Edward J Hu, Yelong Shen, Phillip Wallis, Zeyuan Allen-Zhu, Yanzhi Li, Shean Wang, Lu Wang, and Weizhu Chen. Lora: Low-rank adaptation of large language models. *arXiv preprint arXiv:2106.09685*, 2021.
- Chi-Pin Huang, Kai-Po Chang, Chung-Ting Tsai, Yung-Hsuan Lai, Fu-En Yang, and Yu-Chiang Frank Wang. Receler: Reliable concept erasing of text-to-image diffusion models via lightweight erasers. In *European Conference on Computer Vision*, pp. 360–376. Springer, 2024.
- Anubhav Jain, Yuya Kobayashi, Takashi Shibuya, Yuhta Takida, Nasir Memon, Julian Togelius, and Yuki Mitsufuji. Trasca: Trajectory steering for concept erasure. *arXiv preprint arXiv:2412.07658*, 2024.
- Changhoon Kim, Kyle Min, and Yezhou Yang. Race: Robust adversarial concept erasure for secure text-to-image diffusion model. In *European Conference on Computer Vision*, pp. 461–478. Springer, 2024.
- Diederik Kingma, Tim Salimans, Ben Poole, and Jonathan Ho. Variational diffusion models. *Advances in neural information processing systems*, 34:21696–21707, 2021.
- Yajing Kong, Liu Liu, Zhen Wang, and Dacheng Tao. Balancing stability and plasticity through advanced null space in continual learning. In *European Conference on Computer Vision*, pp. 219–236. Springer, 2022.
- Nupur Kumari, Bingliang Zhang, Sheng-Yu Wang, Eli Shechtman, Richard Zhang, and Jun-Yan Zhu. Ablating concepts in text-to-image diffusion models. In *Proceedings of the IEEE/CVF International Conference on Computer Vision*, pp. 22691–22702, 2023.
- Byung Hyun Lee, Sungjin Lim, and Se Young Chun. Localized concept erasure for text-to-image diffusion models using training-free gated low-rank adaptation. In *Proceedings of the Computer Vision and Pattern Recognition Conference*, pp. 18596–18606, 2025a.
- Byung Hyun Lee, Sungjin Lim, Seunggyu Lee, Dong Un Kang, and Se Young Chun. Concept pinpoint eraser for text-to-image diffusion models via residual attention gate. *arXiv preprint arXiv:2506.22806*, 2025b.
- Ouxiang Li, Yuan Wang, Xinting Hu, Huijuan Huang, Rui Chen, Jiarong Ou, Xin Tao, Pengfei Wan, Xiaojuan Qi, and Fuli Feng. Easier painting than thinking: Can text-to-image models set the stage, but not direct the play? *arXiv preprint arXiv:2509.03516*, 2025.

- Guoliang Lin, Hanlu Chu, and Hanjiang Lai. Towards better plasticity-stability trade-off in incremental learning: A simple linear connector. In *Proceedings of the IEEE/CVF conference on computer vision and pattern recognition*, pp. 89–98, 2022.
- Tsung-Yi Lin, Michael Maire, Serge Belongie, James Hays, Pietro Perona, Deva Ramanan, Piotr Dollár, and C Lawrence Zitnick. Microsoft coco: Common objects in context. In *Computer Vision–ECCV 2014: 13th European Conference, Zurich, Switzerland, September 6–12, 2014, Proceedings, Part V 13*, pp. 740–755. Springer, 2014.
- Cheng Lu, Yuhao Zhou, Fan Bao, Jianfei Chen, Chongxuan Li, and Jun Zhu. Dpm-solver: A fast ode solver for diffusion probabilistic model sampling in around 10 steps. *Advances in Neural Information Processing Systems*, 35:5775–5787, 2022.
- Shilin Lu, Zilan Wang, Leyang Li, Yanzhu Liu, and Adams Wai-Kin Kong. Mace: Mass concept erasure in diffusion models. In *Proceedings of the IEEE/CVF Conference on Computer Vision and Pattern Recognition*, pp. 6430–6440, 2024a.
- Yue Lu, Shizhou Zhang, De Cheng, Yinghui Xing, Nannan Wang, Peng Wang, and Yanning Zhang. Visual prompt tuning in null space for continual learning. *arXiv preprint arXiv:2406.05658*, 2024b.
- Lykon. Dreamshaper v8 model card. <https://huggingface.co/Lykon/dreamshaper-8>, 2023.
- Mengyao Lyu, Yuhong Yang, Haiwen Hong, Hui Chen, Xuan Jin, Yuan He, Hui Xue, Jungong Han, and Guiguang Ding. One-dimensional adapter to rule them all: Concepts diffusion models and erasing applications. In *Proceedings of the IEEE/CVF Conference on Computer Vision and Pattern Recognition*, pp. 7559–7568, 2024.
- Alexander Quinn Nichol and Prafulla Dhariwal. Improved denoising diffusion probabilistic models. In *International conference on machine learning*, pp. 8162–8171. PMLR, 2021.
- OpenAI. OpenAI: Introducing ChatGPT, 2022. URL <https://openai.com/blog/chatgpt>.
- Hadas Orgad, Bahjat Kawar, and Yonatan Belinkov. Editing implicit assumptions in text-to-image diffusion models. In *Proceedings of the IEEE/CVF International Conference on Computer Vision*, pp. 7053–7061, 2023.
- William Peebles and Saining Xie. Scalable diffusion models with transformers. In *Proceedings of the IEEE/CVF International Conference on Computer Vision*, pp. 4195–4205, 2023.
- Dustin Podell, Zion English, Kyle Lacey, Andreas Blattmann, Tim Dockhorn, Jonas Müller, Joe Penna, and Robin Rombach. Sdxl: Improving latent diffusion models for high-resolution image synthesis. *arXiv preprint arXiv:2307.01952*, 2023.
- Alec Radford, Jong Wook Kim, Chris Hallacy, Aditya Ramesh, Gabriel Goh, Sandhini Agarwal, Girish Sastry, Amanda Askell, Pamela Mishkin, Jack Clark, et al. Learning transferable visual models from natural language supervision. In *International conference on machine learning*, pp. 8748–8763. PMLR, 2021.
- Aditya Ramesh, Mikhail Pavlov, Gabriel Goh, Scott Gray, Chelsea Voss, Alec Radford, Mark Chen, and Ilya Sutskever. Zero-shot text-to-image generation. In *International conference on machine learning*, pp. 8821–8831. Pmlr, 2021.
- Javier Rando, Daniel Paleka, David Lindner, Lennart Heim, and Florian Tramèr. Red-teaming the stable diffusion safety filter. *arXiv preprint arXiv:2210.04610*, 2022.
- Dana Rao. Responsible innovation in the age of generative ai, 2023. URL <https://blog.adobe.com/en/publish/2023/03/21/responsible-innovation-age-of-generative-ai>.

- Robin Rombach, Andreas Blattmann, Dominik Lorenz, Patrick Esser, and Björn Ommer. High-resolution image synthesis with latent diffusion models. In *Proceedings of the IEEE/CVF conference on computer vision and pattern recognition*, pp. 10684–10695, 2022.
- Nataniel Ruiz, Yuanzhen Li, Varun Jampani, Yael Pritch, Michael Rubinstein, and Kfir Aberman. Dreambooth: Fine tuning text-to-image diffusion models for subject-driven generation. In *Proceedings of the IEEE/CVF conference on computer vision and pattern recognition*, pp. 22500–22510, 2023.
- Patrick Schramowski, Manuel Brack, Björn Deiseroth, and Kristian Kersting. Safe latent diffusion: Mitigating inappropriate degeneration in diffusion models. In *Proceedings of the IEEE/CVF Conference on Computer Vision and Pattern Recognition*, pp. 22522–22531, 2023.
- Christoph Schuhmann, Richard Vencu, Romain Beaumont, Robert Kaczmarczyk, Clayton Mullis, Aarush Katta, Theo Coombes, Jenia Jitsev, and Aran Komatsuzaki. Laion-400m: Open dataset of clip-filtered 400 million image-text pairs. *arXiv preprint arXiv:2111.02114*, 2021.
- Christoph Schuhmann, Romain Beaumont, Richard Vencu, Cade Gordon, Ross Wightman, Mehdi Cherti, Theo Coombes, Aarush Katta, Clayton Mullis, Mitchell Wortsman, et al. Laion-5b: An open large-scale dataset for training next generation image-text models. *Advances in Neural Information Processing Systems*, 35:25278–25294, 2022.
- SG161222. Realistic vision v5.1 (novae) model card. https://huggingface.co/SG161222/Realistic_Vision_V5.1_noVAE, 2023.
- Shawn Shan, Jenna Cryan, Emily Wenger, Haitao Zheng, Rana Hanocka, and Ben Y Zhao. Glaze: Protecting artists from style mimicry by {Text-to-Image} models. In *32nd USENIX Security Symposium (USENIX Security 23)*, pp. 2187–2204, 2023.
- Jascha Sohl-Dickstein, Eric Weiss, Niru Maheswaranathan, and Surya Ganguli. Deep unsupervised learning using nonequilibrium thermodynamics. In *International Conference on Machine Learning*, pp. 2256–2265. PMLR, 2015.
- Jiaming Song, Chenlin Meng, and Stefano Ermon. Denoising diffusion implicit models. *arXiv preprint arXiv:2010.02502*, 2020a.
- Yang Song, Jascha Sohl-Dickstein, Diederik P Kingma, Abhishek Kumar, Stefano Ermon, and Ben Poole. Score-based generative modeling through stochastic differential equations. *arXiv preprint arXiv:2011.13456*, 2020b.
- Stability AI. Stable diffusion v1-4 model card. <https://huggingface.co/CompVis/stable-diffusion-v1-4>, 2022.
- Yoad Tewel, Rinon Gal, Gal Chechik, and Yuval Atzmon. Key-locked rank one editing for text-to-image personalization. In *ACM SIGGRAPH 2023 Conference Proceedings*, pp. 1–11, 2023.
- Yu-Lin Tsai, Chia-Yi Hsu, Chulin Xie, Chih-Hsun Lin, Jia-You Chen, Bo Li, Pin-Yu Chen, Chia-Mu Yu, and Chun-Ying Huang. Ring-a-bell! how reliable are concept removal methods for diffusion models? *arXiv preprint arXiv:2310.10012*, 2023.
- Aaron Van Den Oord, Oriol Vinyals, et al. Neural discrete representation learning. *Advances in neural information processing systems*, 30, 2017.
- Shipeng Wang, Xiaorong Li, Jian Sun, and Zongben Xu. Training networks in null space of feature covariance for continual learning. In *Proceedings of the IEEE/CVF conference on Computer Vision and Pattern Recognition*, pp. 184–193, 2021.
- Shipeng Wang, Xiaorong Li, Jian Sun, and Zongben Xu. Training networks in null space of feature covariance with self-supervision for incremental learning. *IEEE Transactions on Pattern Analysis and Machine Intelligence*, 2024a.
- Yinhuai Wang, Jiwen Yu, and Jian Zhang. Zero-shot image restoration using denoising diffusion null-space model. *arXiv preprint arXiv:2212.00490*, 2022.

- Yuan Wang, Ouxiang Li, Tingting Mu, Yanbin Hao, Kuiren Liu, Xiang Wang, and Xiangnan He. Precise, fast, and low-cost concept erasure in value space: Orthogonal complement matters. *arXiv preprint arXiv:2412.06143*, 2024b.
- Yuan Wang, Borui Liao, Huijuan Huang, Jinda Lu, Ouxiang Li, Kuiren Liu, Meng Wang, and Xiang Wang. Thinking with frames: Generative video distortion evaluation via frame reward model. *arXiv preprint arXiv:2601.04033*, 2026.
- Zhicai Wang, Ouxiang Li, Tan Wang, Longhui Wei, Yanbin Hao, Xiang Wang, and Qi Tian. Prior preserved text-to-image personalization without image regularization. *IEEE Transactions on Circuits and Systems for Video Technology*, 2024c.
- Yongliang Wu, Shiji Zhou, Mingzhuo Yang, Lianzhe Wang, Heng Chang, Wenbo Zhu, Xinting Hu, Xiao Zhou, and Xu Yang. Unlearning concepts in diffusion model via concept domain correction and concept preserving gradient. In *Proceedings of the AAAI Conference on Artificial Intelligence*, volume 39, pp. 8496–8504, 2025a.
- Yongliang Wu, Yizhou Zhou, Zhou Ziheng, Yingzhe Peng, Xinyu Ye, Xinting Hu, Wenbo Zhu, Lu Qi, Ming-Hsuan Yang, and Xu Yang. On the generalization of sft: A reinforcement learning perspective with reward rectification. *arXiv preprint arXiv:2508.05629*, 2025b.
- Yiyan Xu, Wenjie Wang, Yang Zhang, Biao Tang, Peng Yan, Fuli Feng, and Xiangnan He. Personalized image generation with large multimodal models. In *Proceedings of the ACM on Web Conference 2025*, pp. 264–274, 2025a.
- Yiyan Xu, Jinghao Zhang, Alireza Salemi, Xinting Hu, Wenjie Wang, Fuli Feng, Hamed Zamani, Xiangnan He, and Tat-Seng Chua. Personalized generation in large model era: A survey. In *Proceedings of the 63rd Annual Meeting of the Association for Computational Linguistics (Volume 1: Long Papers)*, pp. 24607–24649, 2025b.
- Shilin Yan, Ouxiang Li, Jiayin Cai, Yanbin Hao, Xiaolong Jiang, Yao Hu, and Weidi Xie. A sanity check for ai-generated image detection. *arXiv preprint arXiv:2406.19435*, 2024.
- Chengyi Yang, Mingda Dong, Xiaoyue Zhang, Jiayin Qi, and Aimin Zhou. Introducing common null space of gradients for gradient projection methods in continual learning. In *Proceedings of the 32nd ACM International Conference on Multimedia*, pp. 5489–5497, 2024a.
- Ling Yang, Zhilong Zhang, Yang Song, Shenda Hong, Runsheng Xu, Yue Zhao, Wentao Zhang, Bin Cui, and Ming-Hsuan Yang. Diffusion models: A comprehensive survey of methods and applications. *ACM Computing Surveys*, 56(4):1–39, 2023.
- Yijun Yang, Ruiyuan Gao, Xiaosen Wang, Tsung-Yi Ho, Nan Xu, and Qiang Xu. Mma-diffusion: Multimodal attack on diffusion models. In *Proceedings of the IEEE/CVF Conference on Computer Vision and Pattern Recognition*, pp. 7737–7746, 2024b.
- Jaehong Yoon, Shoubin Yu, Vaidehi Patil, Huaxiu Yao, and Mohit Bansal. Safree: Training-free and adaptive guard for safe text-to-image and video generation. *arXiv preprint arXiv:2410.12761*, 2024.
- Gong Zhang, Kai Wang, Xingqian Xu, Zhangyang Wang, and Humphrey Shi. Forget-me-not: Learning to forget in text-to-image diffusion models. In *Proceedings of the IEEE/CVF Conference on Computer Vision and Pattern Recognition*, pp. 1755–1764, 2024a.
- Yimeng Zhang, Xin Chen, Jinghan Jia, Yihua Zhang, Chongyu Fan, Jiancheng Liu, Mingyi Hong, Ke Ding, and Sijia Liu. Defensive unlearning with adversarial training for robust concept erasure in diffusion models. *Advances in neural information processing systems*, 37:36748–36776, 2024b.
- Yimeng Zhang, Jinghan Jia, Xin Chen, Aochuan Chen, Yihua Zhang, Jiancheng Liu, Ke Ding, and Sijia Liu. To generate or not? safety-driven unlearned diffusion models are still easy to generate unsafe images... for now. In *European Conference on Computer Vision*, pp. 385–403. Springer, 2024c.

Yimeng Zhang, Jinghan Jia, Xin Chen, Aochuan Chen, Yihua Zhang, Jiancheng Liu, Ke Ding, and Sijia Liu. To generate or not? safety-driven unlearned diffusion models are still easy to generate unsafe images... for now. In *European Conference on Computer Vision*, pp. 385–403. Springer, 2025.

Mengnan Zhao, Lihe Zhang, Xingyi Yang, Tianhang Zheng, and Baocai Yin. Advanchor: Enhancing diffusion model unlearning with adversarial anchors. *arXiv preprint arXiv:2501.00054*, 2024a.

Mengnan Zhao, Lihe Zhang, Tianhang Zheng, Yuqiu Kong, and Baocai Yin. Separable multi-concept erasure from diffusion models. *arXiv preprint arXiv:2402.05947*, 2024b.

A PRELIMINARIES

T2I diffusion models. T2I generation has seen significant advancements with diffusion models, particularly Latent Diffusion Models (LDMs) (Rombach et al., 2022). Unlike pixel-space diffusion, LDMs operate in the latent space of a pretrained autoencoder, reducing computational costs while maintaining high-quality synthesis. LDMs consist of a vector-quantized autoencoder (Van Den Oord et al., 2017; Esser et al., 2021) and a diffusion model (Dhariwal & Nichol, 2021; Ho et al., 2020; Sohl-Dickstein et al., 2015; Kingma et al., 2021; Song et al., 2020b; Wang et al., 2024c; 2026; Li et al., 2025). The autoencoder encodes an image \mathbf{x} into a latent representation $\mathbf{z} = \mathcal{E}(\mathbf{x})$ and reconstructs it via $\mathbf{x} \approx \mathcal{D}(\mathbf{z})$. The diffusion model learns to generate latent codes through a denoising process. The training objective is given by (Ho et al., 2020; Rombach et al., 2022):

$$\mathcal{L}_{\text{LDM}} = \mathbb{E}_{\mathbf{z} \sim \mathcal{E}(\mathbf{x}), \mathbf{c}, \epsilon \sim \mathcal{N}(0,1), t} \left[\|\epsilon - \epsilon_{\theta}(\mathbf{z}_t, t, \mathbf{c})\|_2^2 \right], \quad (13)$$

where \mathbf{z}_t is the noisy latent at timestep t , ϵ is Gaussian noise, ϵ_{θ} is the denoising network, and \mathbf{c} is conditioning information from text, class labels, or segmentation masks (Rombach et al., 2022). During inference, a latent \mathbf{z}_T is sampled from a Gaussian prior and progressively denoised to obtain \mathbf{z}_0 , which is then decoded into an image via $\mathbf{x}_0 \approx \mathcal{D}(\mathbf{z}_0)$.

Cross-attention mechanisms. Current T2I diffusion models usually leverage a generative framework to synthesize images conditioned on textual descriptions in the latent space (Rombach et al., 2022). The conditioning mechanism is implemented through cross-attention (CA) layers. Specifically, textual descriptions are first tokenized into n tokens and embedded into a sequence of vectors $\mathbf{e} \in \mathbb{R}^{d_0 \times n}$ via a pre-trained CLIP model (Radford et al., 2021). These text embeddings serve as the key $\mathbf{K} \in \mathbb{R}^{n \times d_k}$ and value $\mathbf{V} \in \mathbb{R}^{n \times d_v}$ inputs using parametric projection matrices $\mathbf{W}_{\mathbf{K}} \in \mathbb{R}^{d_k \times d_0}$ and $\mathbf{W}_{\mathbf{V}} \in \mathbb{R}^{d_v \times d_0}$, while the intermediate image representations act as the query $\mathbf{Q} \in \mathbb{R}^{m \times d_k}$. The cross-attention mechanism is defined as:

$$\text{Attention}(\mathbf{Q}, \mathbf{K}, \mathbf{V}) = \text{softmax} \left(\frac{\mathbf{Q}\mathbf{K}^T}{\sqrt{d_k}} \right) \mathbf{V}. \quad (14)$$

This alignment enables the model to capture semantic correlations between the textual input and the visual features, ensuring that the generated images are semantically consistent with the provided text prompts.

B PROOF AND DERIVATION

B.1 DERIVING THE CLOSED-FORM SOLUTION FOR UCE

From Eq. 1, we are tasked with minimizing the following editing objective, where the hyperparameters α and β correspond to the weights of the erasure error e_1 and the preservation error e_0 , respectively:

$$\min_{\Delta} \left[\alpha \|\mathbf{W} + \Delta\| \mathbf{C}_1 - \mathbf{W}\mathbf{C}_* \|^2 + \beta \|\Delta\mathbf{C}_0\|^2 \right]. \quad (15)$$

To derive the closed-form solution, we begin by computing the gradient of the objective function with respect to Δ . The gradient is given by:

$$\alpha (\mathbf{W}\mathbf{C}_1 - \mathbf{W}\mathbf{C}_* + \Delta\mathbf{C}_1) \mathbf{C}_1^T + \beta \Delta\mathbf{C}_0\mathbf{C}_0^T = 0. \quad (16)$$

Solving the resulting equation yields the closed-form solution for Δ_{UCE} :

$$\Delta_{\text{UCE}} = \alpha \mathbf{W} (\mathbf{C}_* \mathbf{C}_1^T - \mathbf{C}_1 \mathbf{C}_1^T) (\alpha \mathbf{C}_1 \mathbf{C}_1^T + \beta \mathbf{C}_0 \mathbf{C}_0^T)^{-1}. \quad (17)$$

In practice, an additional identity matrix \mathbf{I} with hyperparameter λ is added to $(\alpha \mathbf{C}_1 \mathbf{C}_1^T + \beta \mathbf{C}_0 \mathbf{C}_0^T)^{-1}$ to ensure its invertibility. This modification results in the following closed-form solution for UCE:

$$\Delta_{\text{UCE}} = \alpha \mathbf{W} (\mathbf{C}_* \mathbf{C}_1^T - \mathbf{C}_1 \mathbf{C}_1^T) (\alpha \mathbf{C}_1 \mathbf{C}_1^T + \beta \mathbf{C}_0 \mathbf{C}_0^T + \lambda \mathbf{I})^{-1}. \quad (18)$$

B.2 PROOF OF THE LOWER BOUND OF e_0 FOR UCE

Herein, we aim to establish the existence of a strictly positive constant $c > 0$ such that

$$e_0 = \|\Delta_{\text{UCE}} \mathbf{C}_0\|^2 = \|\alpha \mathbf{W} (\mathbf{C}_* \mathbf{C}_1^\top - \mathbf{C}_1 \mathbf{C}_1^\top) (\alpha \mathbf{C}_1 \mathbf{C}_1^\top + \beta \mathbf{C}_0 \mathbf{C}_0^\top + \lambda \mathbf{I})^{-1} \mathbf{C}_0\|^2 \geq c > 0. \quad (19)$$

Assumption B.1. We assume that $\alpha, \beta, \lambda \neq 0$, that \mathbf{W} is a full-rank matrix, and that $\mathbf{C}_0 \mathbf{C}_0^\top$ is rank-deficient. Furthermore, we assume that

$$\mathbf{C}_* \mathbf{C}_1^\top - \mathbf{C}_1 \mathbf{C}_1^\top \neq \mathbf{0}.$$

Proof. Define the matrix \mathbf{M} as

$$\mathbf{M} = \alpha \mathbf{C}_1 \mathbf{C}_1^\top + \beta \mathbf{C}_0 \mathbf{C}_0^\top + \lambda \mathbf{I}. \quad (20)$$

Since $\lambda > 0$ and \mathbf{I} is positive definite, it follows that \mathbf{M} is strictly positive definite and therefore invertible.

Rewriting e_0 by defining $\mathbf{B} = \mathbf{M}^{-1} \mathbf{C}_0$, we obtain

$$e_0 = \|\alpha \mathbf{W} (\mathbf{C}_* \mathbf{C}_1^\top - \mathbf{C}_1 \mathbf{C}_1^\top) \mathbf{B}\|^2. \quad (21)$$

Applying the singular value bound for matrix products, we have

$$\|\mathbf{X}\mathbf{Y}\| \geq \sigma_{\min}(\mathbf{X}) \|\mathbf{Y}\|, \quad (22)$$

where $\sigma_{\min}(\mathbf{X})$ is the smallest singular value of \mathbf{X} . Applying this inequality, we obtain

$$\|\mathbf{W} (\mathbf{C}_* \mathbf{C}_1^\top - \mathbf{C}_1 \mathbf{C}_1^\top) \mathbf{B}\| \geq \sigma_{\min}(\mathbf{W}) \|(\mathbf{C}_* \mathbf{C}_1^\top - \mathbf{C}_1 \mathbf{C}_1^\top) \mathbf{B}\|. \quad (23)$$

We start with the singular value decomposition (SVD) of the matrix $\mathbf{C}_* \mathbf{C}_1^\top - \mathbf{C}_1 \mathbf{C}_1^\top$, given by

$$\mathbf{C}_* \mathbf{C}_1^\top - \mathbf{C}_1 \mathbf{C}_1^\top = \mathbf{U} \mathbf{\Sigma} \mathbf{V}^\top. \quad (24)$$

Here, \mathbf{U} and \mathbf{V} are orthogonal matrices, and

$$\mathbf{\Sigma} = \text{diag}(\sigma_1, \sigma_2, \dots, \sigma_r, 0, \dots, 0) \quad (25)$$

is a diagonal matrix containing the singular values $\sigma_1 \geq \sigma_2 \geq \dots \geq \sigma_r > 0$, followed by zeros.

Multiplying both sides by \mathbf{B} , we obtain

$$(\mathbf{C}_* \mathbf{C}_1^\top - \mathbf{C}_1 \mathbf{C}_1^\top) \mathbf{B} = \mathbf{U} \mathbf{\Sigma} \mathbf{V}^\top \mathbf{B}. \quad (26)$$

Define the projection of \mathbf{B} onto the subspace spanned by the right singular vectors as

$$\mathbf{B}_{\text{proj}} = \mathbf{V}^\top \mathbf{B}. \quad (27)$$

Then, we can rewrite the expression as

$$(\mathbf{C}_* \mathbf{C}_1^\top - \mathbf{C}_1 \mathbf{C}_1^\top) \mathbf{B} = \mathbf{U} \mathbf{\Sigma} \mathbf{B}_{\text{proj}}. \quad (28)$$

Taking norms on both sides and using the fact that orthogonal transformations preserve norms, we get

$$\|(\mathbf{C}_* \mathbf{C}_1^\top - \mathbf{C}_1 \mathbf{C}_1^\top) \mathbf{B}\| = \|\mathbf{\Sigma} \mathbf{B}_{\text{proj}}\|. \quad (29)$$

Since $\mathbf{\Sigma}$ is a diagonal matrix, its smallest nonzero singular value σ_r provides a lower bound:

$$\|\mathbf{\Sigma} \mathbf{B}_{\text{proj}}\| \geq \sigma_r \|\mathbf{B}_{\text{proj}}\|. \quad (30)$$

Next, we establish a lower bound for $\|\mathbf{B}_{\text{proj}}\|$. Given that \mathbf{V} is composed of right singular vectors, there exists a smallest non-zero singular value c_1 such that:

$$\|\mathbf{B}_{\text{proj}}\| \geq c_1 \|\mathbf{B}\|. \quad (31)$$

Combining these inequalities, we obtain

$$\|(\mathbf{C}_* \mathbf{C}_1^\top - \mathbf{C}_1 \mathbf{C}_1^\top) \mathbf{B}\| \geq \sigma_r \|\mathbf{B}_{\text{proj}}\| \geq \sigma_r c_1 \|\mathbf{B}\|. \quad (32)$$

Since \mathbf{M} is positive definite, we use the standard norm inequality for an invertible matrix \mathbf{M} , which states that for any matrix \mathbf{X} ,

$$\|\mathbf{M}\mathbf{X}\| \leq \|\mathbf{M}\|\|\mathbf{X}\|. \quad (33)$$

Setting $\mathbf{X} = \mathbf{M}^{-1}\mathbf{C}_0$, we obtain

$$\|\mathbf{M}\mathbf{M}^{-1}\mathbf{C}_0\| \leq \|\mathbf{M}\|\|\mathbf{M}^{-1}\mathbf{C}_0\|. \quad (34)$$

Since $\mathbf{M}\mathbf{M}^{-1} = \mathbf{I}$, the left-hand side simplifies to $\|\mathbf{C}_0\|$, yielding

$$\|\mathbf{C}_0\| \leq \|\mathbf{M}\|\|\mathbf{M}^{-1}\mathbf{C}_0\|. \quad (35)$$

Dividing both sides by $\|\mathbf{M}\|$, we obtain

$$\|\mathbf{M}^{-1}\mathbf{C}_0\| \geq \frac{1}{\|\mathbf{M}\|}\|\mathbf{C}_0\|. \quad (36)$$

Thus, it follows that

$$\|\mathbf{B}\| = \|\mathbf{M}^{-1}\mathbf{C}_0\| \geq \frac{1}{\|\mathbf{M}\|}\|\mathbf{C}_0\|. \quad (37)$$

Combining the above results, we obtain

$$\|\mathbf{W}(\mathbf{C}_*\mathbf{C}_1^\top - \mathbf{C}_1\mathbf{C}_1^\top)\mathbf{B}\| \geq \sigma_{\min}(\mathbf{W})\sigma_r c_1 \frac{1}{\|\mathbf{M}\|}\|\mathbf{C}_0\|. \quad (38)$$

Squaring both sides, we conclude that

$$e_0 = \|\alpha\mathbf{W}(\mathbf{C}_*\mathbf{C}_1^\top - \mathbf{C}_1\mathbf{C}_1^\top)\mathbf{B}\|^2 \geq \alpha^2\sigma_{\min}^2(\mathbf{W})\sigma_r^2 c_1^2 \frac{1}{\|\mathbf{M}\|^2}\|\mathbf{C}_0\|^2. \quad (39)$$

Since all terms on the right-hand side are strictly positive by assumption, we establish the existence of a positive lower bound $c > 0$ such that

$$e_0 \geq c > 0. \quad (40)$$

This completes the proof. \square

B.3 DERIVING THE CLOSED-FORM SOLUTION FOR SPEED

From Eq. 10, we are tasked with minimizing the following editing objective:

$$\min_{\Delta} \|(\mathbf{W} + \Delta\mathbf{P})\mathbf{C}_1 - \mathbf{W}\mathbf{C}_*\|^2 + \|\Delta\mathbf{P}\|^2, \quad \text{s.t. } (\Delta\mathbf{P})\mathbf{C}_2 = \mathbf{0}. \quad (41)$$

This is a weighted least squares problem subject to an equality constraint. To solve it, we first formulate the Lagrangian function, where Λ is the Lagrange multiplier:

$$\mathcal{L}(\Delta, \Lambda) = \|(\mathbf{W} + \Delta\mathbf{P})\mathbf{C}_1 - \mathbf{W}\mathbf{C}_*\|^2 + \|\Delta\mathbf{P}\|^2 + \Lambda^\top ((\Delta\mathbf{P})\mathbf{C}_2). \quad (42)$$

We compute the gradient of the Lagrangian function in Eq. 42 with respect to Δ and set it to zero, yielding the following equation for Δ :

$$\frac{\partial \mathcal{L}(\Delta, \Lambda)}{\partial \Delta} = 2((\mathbf{W} + \Delta\mathbf{P})\mathbf{C}_1 - \mathbf{W}\mathbf{C}_*)\mathbf{C}_1^\top \mathbf{P}^\top + 2\Delta\mathbf{P}\mathbf{P}^\top + \Lambda\mathbf{C}_2^\top \mathbf{P}^\top = \mathbf{0}. \quad (43)$$

Given that the projection matrix \mathbf{P} is derived from R_{refine} using Eq. 2, \mathbf{P} is a symmetric matrix (*i.e.*, $\mathbf{P} = \mathbf{P}^\top$) and an idempotent matrix (*i.e.*, $\mathbf{P}^2 = \mathbf{P}$), the above formulation can be simplified to:

$$\frac{\partial \mathcal{L}(\Delta, \Lambda)}{\partial \Delta} = 2((\mathbf{W} + \Delta\mathbf{P})\mathbf{C}_1 - \mathbf{W}\mathbf{C}_*)\mathbf{C}_1^\top \mathbf{P} + 2\Delta\mathbf{P} + \Lambda\mathbf{C}_2^\top \mathbf{P} = \mathbf{0}. \quad (44)$$

Therefore, we can obtain the closed-form solution for $\Delta\mathbf{P}$ from this equation:

$$\Delta\mathbf{P} = (\mathbf{W}\mathbf{C}_*\mathbf{C}_1^\top \mathbf{P} - \mathbf{W}\mathbf{C}_1\mathbf{C}_1^\top \mathbf{P} - \frac{1}{2}\Lambda\mathbf{C}_2^\top \mathbf{P})(\mathbf{C}_1\mathbf{C}_1^\top \mathbf{P} + \mathbf{I})^{-1}. \quad (45)$$

Table 4: **Evaluation setup for multi-concept erasure.** This dataset contains an erasure set with 100 celebrities and a retain set with another 100 celebrities. We experiment with erasing 10, 50, and 100 celebrities with the predefined target concepts and the entire retain set is utilized in all cases.

Group	Number	Anchor Concept	Celebrity
Erasure Set	10	'person'	'Adam Driver', 'Adriana Lima', 'Amber Heard', 'Amy Adams', 'Andrew Garfield', 'Angelina Jolie', 'Anjelica Huston', 'Anna Faris', 'Anna Kendrick', 'Anne Hathaway'
	50	'person'	'Adam Driver', 'Adriana Lima', 'Amber Heard', 'Amy Adams', 'Andrew Garfield', 'Angelina Jolie', 'Anjelica Huston', 'Anna Faris', 'Anna Kendrick', 'Anne Hathaway', 'Arnold Schwarzenegger', 'Barack Obama', 'Beth Behrs', 'Bill Clinton', 'Bob Dylan', 'Bob Marley', 'Bradley Cooper', 'Bruce Willis', 'Bryan Cranston', 'Cameron Diaz', 'Channing Tatum', 'Charlie Sheen', 'Charlize Theron', 'Chris Evans', 'Chris Hemsworth', 'Chris Pine', 'Chuck Norris', 'Courteney Cox', 'Demi Lovato', 'Drake', 'Drew Barrymore', 'Dwayne Johnson', 'Ed Sheeran', 'Elon Musk', 'Elvis Presley', 'Emma Stone', 'Frida Kahlo', 'George Clooney', 'Glenn Close', 'Gwyneth Paltrow', 'Harrison Ford', 'Hillary Clinton', 'Hugh Jackman', 'Idris Elba', 'Jake Gyllenhaal', 'James Franco', 'Jared Leto', 'Jason Momoa', 'Jennifer Aniston', 'Jennifer Lawrence'
	100	'person'	'Adam Driver', 'Adriana Lima', 'Amber Heard', 'Amy Adams', 'Andrew Garfield', 'Angelina Jolie', 'Anjelica Huston', 'Anna Faris', 'Anna Kendrick', 'Anne Hathaway', 'Arnold Schwarzenegger', 'Barack Obama', 'Beth Behrs', 'Bill Clinton', 'Bob Dylan', 'Bob Marley', 'Bradley Cooper', 'Bruce Willis', 'Bryan Cranston', 'Cameron Diaz', 'Channing Tatum', 'Charlie Sheen', 'Charlize Theron', 'Chris Evans', 'Chris Hemsworth', 'Chris Pine', 'Chuck Norris', 'Courteney Cox', 'Demi Lovato', 'Drake', 'Drew Barrymore', 'Dwayne Johnson', 'Ed Sheeran', 'Elon Musk', 'Elvis Presley', 'Emma Stone', 'Frida Kahlo', 'George Clooney', 'Glenn Close', 'Gwyneth Paltrow', 'Harrison Ford', 'Hillary Clinton', 'Hugh Jackman', 'Idris Elba', 'Jake Gyllenhaal', 'James Franco', 'Jared Leto', 'Jason Momoa', 'Jennifer Aniston', 'Jennifer Lawrence', 'Jennifer Lopez', 'Jeremy Renner', 'Jessica Biel', 'Jessica Chastain', 'John Oliver', 'John Wayne', 'Johnny Depp', 'Julianne Hough', 'Justin Timberlake', 'Kate Bosworth', 'Kate Winslet', 'Leonardo DiCaprio', 'Maggie Gyllenhaal', 'Mariah Carey', 'Melania Trump', 'Meryl Streep', 'Mick Jagger', 'Mila Kunis', 'Milla Jovovich', 'Morgan Freeman', 'Nick Jonas', 'Nicolas Cage', 'Nicole Kidman', 'Octavia Spencer', 'Olivia Wilde', 'Oprah Winfrey', 'Paul McCartney', 'Paul Walker', 'Peter Dinklage', 'Philip Seymour Hoffman', 'Reese Witherspoon', 'Richard Gere', 'Ricky Gervais', 'Rihanna', 'Robin Williams', 'Ronald Reagan', 'Ryan Gosling', 'Ryan Reynolds', 'Shia Labeouf', 'Shirley Temple', 'Spike Lee', 'Stan Lee', 'Theresa May', 'Tom Cruise', 'Tom Hanks', 'Tom Hardy', 'Tom Hiddleston', 'Whoopi Goldberg', 'Zac Efron', 'Zayn Malik'
Retain Set	10, 50, and 100	-	'Aaron Paul', 'Alec Baldwin', 'Amanda Seyfried', 'Amy Poehler', 'Amy Schumer', 'Amy Winehouse', 'Andy Samberg', 'Aretha Franklin', 'Avril Lavigne', 'Aziz Ansari', 'Barry Manilow', 'Ben Affleck', 'Ben Stiller', 'Benicio Del Toro', 'Bette Midler', 'Betty White', 'Bill Murray', 'Bill Nye', 'Britney Spears', 'Brittany Snow', 'Bruce Lee', 'Burt Reynolds', 'Charles Manson', 'Christie Brinkley', 'Christina Hendricks', 'Clint Eastwood', 'Countess Vaughn', 'Dakota Johnson', 'Dane DeHaan', 'David Bowie', 'David Tennant', 'Denise Richards', 'Doris Day', 'Dr Dre', 'Elizabeth Taylor', 'Emma Roberts', 'Fred Rogers', 'Gal Gadot', 'George Bush', 'George Takei', 'Gillian Anderson', 'Gordon Ramsey', 'Halle Berry', 'Harry Dean Stanton', 'Harry Styles', 'Hayley Atwell', 'Heath Ledger', 'Henry Cavill', 'Jackie Chan', 'Jada Pinkett Smith', 'James Garner', 'Jason Statham', 'Jeff Bridges', 'Jennifer Connelly', 'Jensen Ackles', 'Jim Morrison', 'Jimmy Carter', 'Joan Rivers', 'John Lennon', 'Johnny Cash', 'Jon Hamm', 'Judy Garland', 'Julianne Moore', 'Justin Bieber', 'Kaley Cuoco', 'Kate Upton', 'Keanu Reeves', 'Kim Jong Un', 'Kirsten Dunst', 'Kristen Stewart', 'Krysten Ritter', 'Lana Del Rey', 'Leslie Jones', 'Lily Collins', 'Lindsay Lohan', 'Liv Tyler', 'Lizzy Caplan', 'Maggie Gyllenhaal', 'Matt Damon', 'Matt Smith', 'Matthew McConaughey', 'Maya Angelou', 'Megan Fox', 'Mel Gibson', 'Melanie Griffith', 'Michael Cera', 'Michael Ealy', 'Natalie Portman', 'Neil Degrasse Tyson', 'Niall Horan', 'Patrick Stewart', 'Paul Rudd', 'Paul Wesley', 'Pierce Brosnan', 'Prince', 'Queen Elizabeth', 'Rachel Dratch', 'Rachel McAdams', 'Reba McEntire', 'Robert De Niro'

Next, we differentiate the Lagrangian function in Eq. 42 with respect to Λ and set it to zero:

$$\frac{\partial \mathcal{L}(\Delta, \Lambda)}{\partial \Lambda} = (\Delta \mathbf{P}) \mathbf{C}_2 = \mathbf{0}. \quad (46)$$

For simplicity, we define $\mathbf{M} = (\mathbf{C}_1 \mathbf{C}_1^\top \mathbf{P} + \mathbf{I})^{-1}$. Then, we substitute the result of Eq. 45 into Eq. 46 and obtain:

$$(\mathbf{W} \mathbf{C}_* \mathbf{C}_1^\top \mathbf{P} - \mathbf{W} \mathbf{C}_1 \mathbf{C}_1^\top \mathbf{P} - \frac{1}{2} \Lambda \mathbf{C}_2^\top \mathbf{P}) \mathbf{M} \mathbf{C}_2 = \mathbf{0}. \quad (47)$$

Solving this equation leads to:

$$\frac{1}{2} \Lambda = \mathbf{W} (\mathbf{C}_* \mathbf{C}_1^\top - \mathbf{C}_1 \mathbf{C}_1^\top) \mathbf{P} \mathbf{M} \mathbf{C}_2 (\mathbf{C}_2^\top \mathbf{P} \mathbf{M} \mathbf{C}_2)^{-1}. \quad (48)$$

Substituting Eq. 48 back into Eq. 45, we have the closed-form solution of our objective:

$$(\Delta \mathbf{P})_{\text{SPEED}} = \mathbf{W} (\mathbf{C}_* \mathbf{C}_1^\top - \mathbf{C}_1 \mathbf{C}_1^\top) \mathbf{P} \mathbf{Q} \mathbf{M}, \quad (49)$$

where $\mathbf{Q} = \mathbf{I} - \mathbf{M} \mathbf{C}_2 (\mathbf{C}_2^\top \mathbf{P} \mathbf{M} \mathbf{C}_2)^{-1} \mathbf{C}_2^\top \mathbf{P}$ and $\mathbf{M} = (\mathbf{C}_1 \mathbf{C}_1^\top \mathbf{P} + \mathbf{I})^{-1}$.

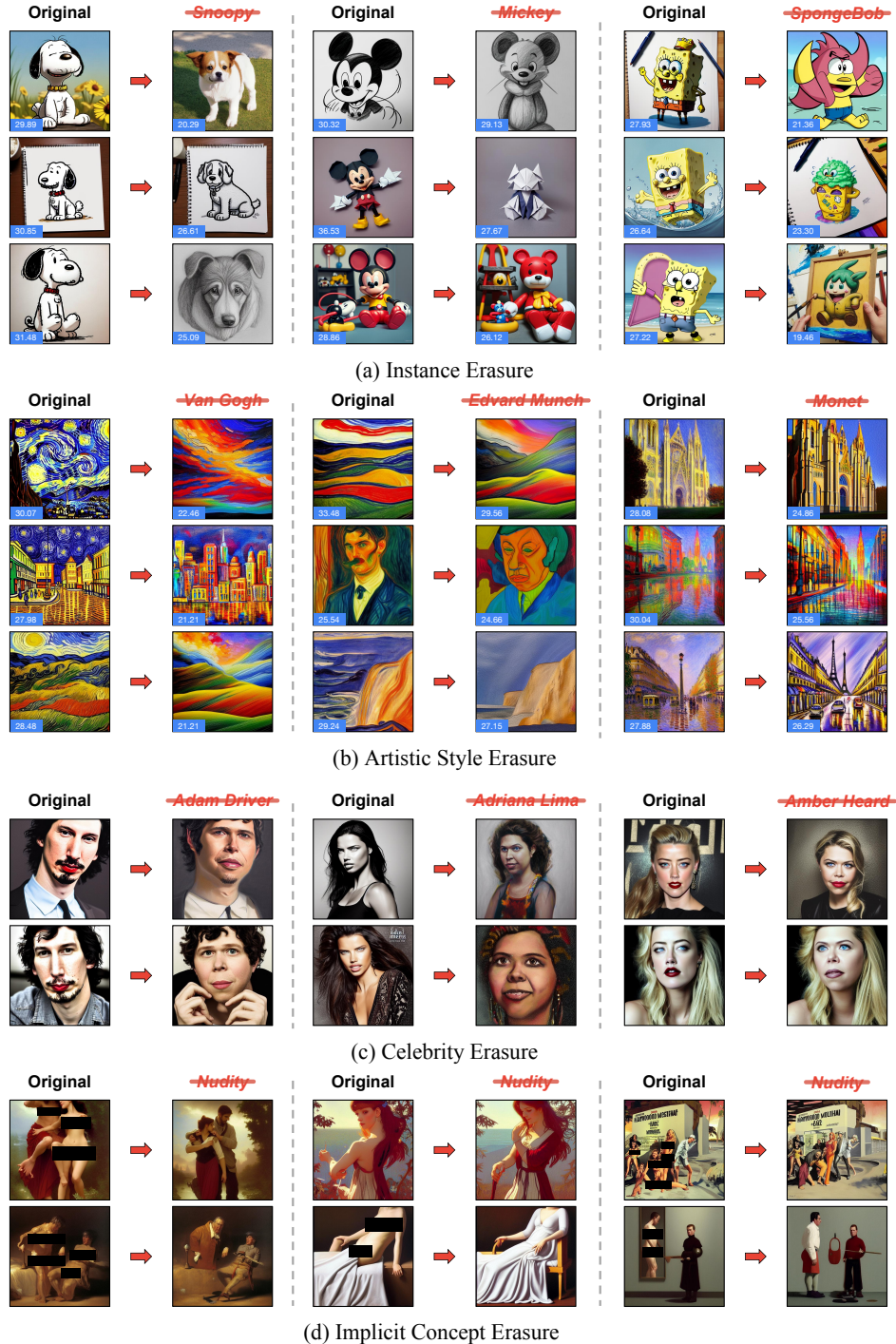


Figure 7: **Qualitative demonstration of our erasure performance** across (a) *instance erasure*, (b) *artistic style erasure*, (c) *celebrity erasure*, and (d) *implicit concept erasure*. Our method achieves effective erasure efficacy across various scenarios while exhibiting superior prior preservation. The corresponding CS is highlighted in blue, indicating that successful erasure can be achieved without pushing CS much lower, as our results demonstrate sufficient erasure at a moderate level.

C IMPLEMENTATION DETAILS

C.1 EXPERIMENTAL SETUP DETAILS

Few-concept erasure. We first compare methods on few-concept erasure, a fundamental concept erasure task, including both instance erasure and artistic style erasure following (Lyu et al., 2024). For instance erasure, we prepare 80 instance templates proposed in CLIP (Radford et al., 2021), such as “*a photo of the {Instance}*”, “*a drawing of the {Instance}*”, and “*a painting of the {Instance}*”. For artistic style erasure, we use ChatGPT (OpenAI, 2022; Achiam et al., 2023) to generate 30 artistic style templates, including “*{Artistic} style painting of the night sky with bold strokes*”, “*{Artistic} style landscape of rolling hills with dramatic brushwork*”, and “*Sunrise scene in {Artistic} style, capturing the beauty of dawn*”. Following (Lyu et al., 2024), we handpick the representative target and anchor concepts as the erasure set (i.e., *Snoopy, Mickey, Spongebob* → ‘ ’ in instance erasure and *Van Gogh, Picasso, Monet* → ‘art’ in artistic style erasure) and non-target concepts for evaluation (i.e., *Pikachu* and *Hello Kitty* in instance erasure and *Paul Gauguin* and *Caravaggio* in artistic style erasure). In terms of the retain set, for instance erasure, we use a scraping script to crawl Wikipedia category pages to extract fictional character names and their page view counts with a threshold of 500,000 views from 2020.01.01 to 2023.12.31, resulting in 1,352 instances. For artistic style erasure, we use the 1,734 artistic styles collected from UCE (Gandikota et al., 2024). In evaluation, we generate 10 images per template per concept, resulting in 800 and 300 images for each concept in instance erasure and artistic style erasure, respectively. Moreover, we introduce the MS-COCO captions (Lin et al., 2014) to serve as general prior knowledge. In implementation, we use the first 1,000 captions to generate a total of 1000 images to compare CS and FID before and after erasure.

Multi-concept erasure. We then compare methods on multi-concept erasure, a more challenging and realistic concept erasure task. Following the experiment setup from (Lu et al., 2024a), we introduce a dataset consisting of 200 celebrities, where their portraits generated by SDv1.4 (Stability AI, 2022) can be recognizable with exceptional accuracy by the GIPHY Celebrity Detector (GCD) (Hasty et al., 2019). This dataset is divided into two groups: an erasure set with 10, 50, and 100 celebrities and a retain set with 100 other celebrities. The full list for both sets is presented in Table 4. We experiment with erasing 10, 50, and 100 celebrities with the predefined target concepts and the entire retain set is utilized in all cases. In evaluation, we prepare five celebrity templates, (i.e., “*a portrait of {Celebrity}*”, “*a sketch of {Celebrity}*”, “*an oil painting of {Celebrity}*”, “*{Celebrity} in an official photo*”, and “*an image capturing {Celebrity} at a public event*”) and generate 500 images for both sets. For non-target concepts, we generate 1 image per template for each of the 100 concepts, totaling 500 images. For target concepts, we adjust the per-concept quantity to maintain a total of 500 images (e.g., erasing 10 celebrities involves generating 10 images with 5 templates).

C.2 ERASURE CONFIGURATIONS

Implementation of previous works. In our series of three concept erasure tasks, we mainly compare against four methods: ConAbl⁴ (Kumari et al., 2023), MACE⁵ (Lu et al., 2024a), RECE⁶ (Gong et al., 2025), and UCE⁷ (Gandikota et al., 2024), as they achieve SOTA performance across different concept erasure tasks. All the compared methods are implemented using their default configurations from the corresponding official repositories. One exception is that for MACE when erasing 50 celebrities, since it doesn’t provide an official configuration and the *preserve weight* varies with the number of target celebrities, we set it to 1.2×10^5 to ensure a consistent balance between concept erasure and prior preservation.

Implementation of SPEED. In line with previous methods (Kumari et al., 2023; Lu et al., 2024a; Wu et al., 2025b; Gong et al., 2025; Gandikota et al., 2024), we edit the cross-attention (CA) layers within the diffusion model due to their role in text-image alignment (Hertz et al., 2022). In contrast, we only edit the value matrices in the CA layers, as suggested by (Wang et al., 2024b). This choice is grounded in the observation that the keys in CA layers typically govern the layout and compositional

⁴<https://github.com/nupurkmr9/concept-ablation>

⁵<https://github.com/Shilin-LU/MACE>

⁶<https://github.com/CharlesGong12/RECE>

⁷<https://github.com/rohitgandikota/unified-concept-editing>

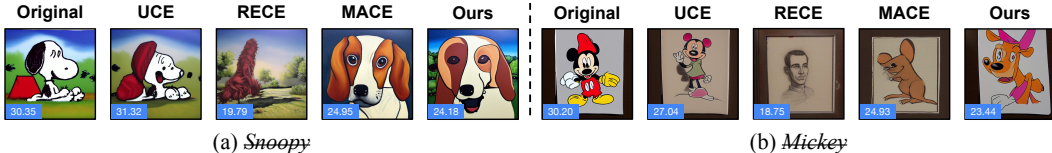


Figure 8: **Comparison of CS values across different erasure methods.** We compare the results in erasing *Snoopy* and *Mickey*, and highlight the corresponding CS in blue. Our method achieves successful concept erasure with moderate CS values. In contrast, RECE achieves the lowest CS by enabling more aggressive erasure. For example, removing *Snoopy* into a landscape without a subject, and changing *Mickey* into a generic person. We argue that such over-erase unnecessarily compromises prior preservation as evidenced by Tables 1 and 2.

structure of the attention map, while the values control the content and visual appearance of the images (Tewel et al., 2023). In the context of concept erasure, our goal is to effectively remove the semantics of the target concept, and we find that only editing the value matrices is sufficient in Figs. 4 and 5, which is quantitatively ablated in Appx. D.5. The augmentation times N_A in Eq. 9 is set to 10 and the augmentation ranks r in Eq. 7 is set to 1 as ablated in Appx. D.5. Meanwhile, given that eigenvalues are rarely strictly zero in practical applications when determining the null space, we select the singular vectors corresponding to the singular values below 10^{-1} on few-concept and implicit concept erasure and 10^{-4} on multi-concept erasure following (Fang et al., 2024).

D ADDITIONAL EXPERIMENTS

D.1 MORE DEMONSTRATIONS

We further provide qualitative visualizations of the erasure results in Fig. 7, illustrating the effectiveness of our method in performing precise and targeted concept erasure across diverse scenarios. Specifically, we showcase: (a) *instance erasure* from Table 1 (left); (b) *artistic style erasure* from Table 1 (right); (c) *celebrity erasure* from Table 2; and (d) *implicit concept erasure* (e.g., *nudity*) from Table 9. In all cases, our method successfully removes the intended concept while preserving unrelated content, demonstrating its universal erasure applications.

We also evaluate the CS value before and after concept erasure to assess the erasure efficacy. As shown in Fig. 8, our method achieves successful erasure of specific concepts such as *Snoopy* and *Mickey* while maintaining moderate CS values (24.18 and 23.44, respectively). This indicates that effective erasure does not require minimizing CS to an extreme.

In contrast, RECE obtains the lowest CS (19.76 and 18.75), but this is achieved at the cost of overly aggressive erasure. For example, transforming *Snoopy* into an unrecognizable image and replacing *Mickey* with a generic human figure. While such strategies may enhance erasure efficacy, they also risk compromising prior knowledge. This trade-off is reflected in higher non-target FIDs, as shown in Tables 1 and 2.

To further demonstrate that our current erasure is adequate, we additionally conduct a human study. For our method and RECE, we randomly sample 50 generated images per method to erase *Snoopy*, *Mickey*, and *Spongebob*. We then recruit 30 human participants through Amazon Mechanical Turk (Amazon) to vote “yes” or “no” on whether the target concept is visually erased or not. As shown in Table 5, the overall results (RECE’s 98.76% v.s. Our 98.47%) indicate that our method achieves successful erasure on par with RECE from the human perspective.

D.2 COMPLETE RESULTS ON FEW-CONCEPT ERASURE

We present complete quantitative comparisons of few-concept erasure, including both CS and FID, in Table 6 and Table 7. Our results demonstrate that our method consistently achieves superior prior preservation, as indicated by higher CS and lower FID across the majority of non-target concepts.

Table 5: **Human study** of erasure efficacy in erasing *Snoopy*, *Mickey*, and *Spongebob* from Table 1.

	<i>Snoopy</i>	<i>Mickey</i>	<i>Spongebob</i>	Average
RECE	98.93%	98.27%	99.07%	98.76%
Ours	98.20%	98.40%	98.80%	98.47%

Table 6: **Complete quantitative comparison of the few-concept erasure** in erasing instances from Table 1 (left). The best results are highlighted in **bold**, and grey columns are indirect indicators for measuring erasure efficacy on target concepts or prior preservation on non-target concepts.

	Snoopy		Mickey		Spongebob		Pikachu		Hello Kitty		MS-COCO	
	CS	FID	CS	FID	CS	FID	CS	FID	CS	FID	CS	FID
SD v1.4	28.51	-	26.62	-	27.30	-	27.44	-	27.77	-	26.53	-
Erase <i>Snoopy</i>												
	CS ↓	FID ↑	CS ↑	FID ↓	CS ↑	FID ↓	CS ↑	FID ↓	CS ↑	FID ↓	CS ↑	FID ↓
ConAbl	25.44	98.38	26.63	37.08	26.95	38.92	27.47	26.14	27.65	36.52	26.40	21.20
MACE	20.90	165.74	23.46	105.97	23.35	102.77	26.05	65.71	26.05	75.42	26.09	42.62
RECE	18.38	151.46	26.62	26.63	27.23	34.42	27.47	21.99	27.78	32.35	26.39	25.61
UCE	23.19	102.86	26.64	24.87	27.29	29.86	27.47	19.06	27.75	27.86	26.46	22.18
SPM	23.72	116.26	26.62	31.21	27.21	31.96	27.41	19.82	27.80	30.95	26.47	20.71
SPM w/o FT	23.72	116.26	26.55	43.03	26.84	42.96	27.38	25.95	27.71	42.53	26.48	20.86
Ours	23.50	108.51	26.67	23.41	27.31	24.64	27.48	16.81	27.82	21.74	26.48	19.95
Erase <i>Snoopy</i> and <i>Mickey</i>												
	CS ↓	FID ↑	CS ↓	FID ↑	CS ↑	FID ↓	CS ↑	FID ↓	CS ↑	FID ↓	CS ↑	FID ↓
ConAbl	25.26	106.78	26.58	57.05	26.81	45.08	27.34	35.57	27.74	41.48	26.42	24.34
MACE	20.53	170.01	20.63	142.98	22.03	112.01	24.98	91.72	23.64	106.88	25.50	55.15
RECE	18.57	150.84	19.14	145.59	27.29	35.85	27.37	26.05	27.71	40.77	26.31	30.30
UCE	23.60	99.30	24.79	86.32	27.32	30.58	27.38	23.51	27.74	31.76	26.38	26.06
SPM	23.18	122.17	22.71	117.30	26.92	38.35	27.35	27.13	27.76	39.61	26.45	24.59
SPM w/o FT	22.45	127.95	21.77	127.57	25.96	61.52	27.39	42.63	27.14	68.75	26.43	23.82
Ours	23.58	103.62	23.62	83.70	27.34	29.67	27.39	22.51	27.78	28.23	26.47	23.66
Erase <i>Snoopy</i> and <i>Mickey</i> and <i>Spongebob</i>												
	CS ↓	FID ↑	CS ↓	FID ↑	CS ↓	FID ↑	CS ↑	FID ↓	CS ↑	FID ↓	CS ↑	FID ↓
ConAbl	24.92	112.66	26.46	63.95	25.12	102.68	27.36	46.47	27.72	48.24	26.37	26.71
MACE	19.86	175.43	19.35	140.13	20.12	143.17	19.76	110.12	21.03	128.56	23.39	66.39
RECE	18.17	155.26	18.87	149.77	16.23	178.55	27.34	40.52	27.71	52.06	26.32	32.51
UCE	23.29	101.40	24.63	88.11	19.08	140.40	27.45	29.20	27.82	38.15	26.30	28.71
SPM	22.86	125.66	22.08	123.20	20.92	153.36	27.45	37.51	27.63	46.63	26.48	25.47
SPM w/o FT	21.80	137.98	20.86	139.48	20.19	163.21	26.68	66.15	26.24	85.35	26.33	25.05
Ours	23.69	103.33	23.93	86.55	21.39	109.28	27.47	21.40	27.76	26.22	26.51	24.99

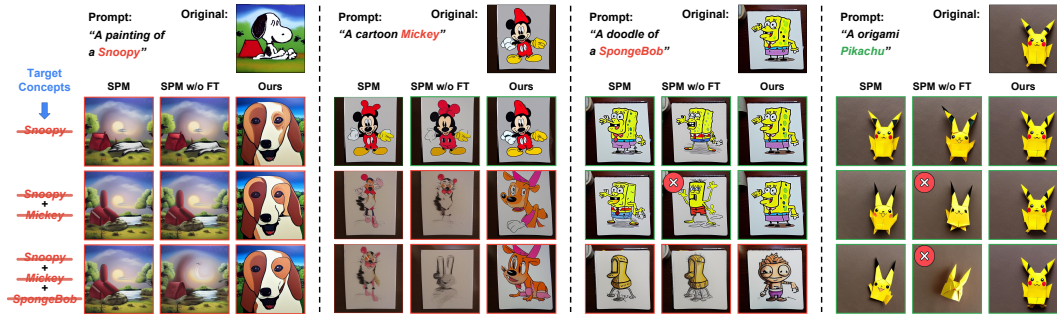


Figure 9: **Qualitative comparison with SPM and SPM w/o FT** in erasing single and multiple instances. The erased and preserved generations are highlighted with **red** and **green** boxes, respectively. Our method demonstrates superior prior preservation compared to both baselines. Meanwhile, without *Facilitated Transport*, SPM w/o FT shows poorer prior preservation in multi-concept erasure (e.g., marked by ⊗) with significant semantic changes compared to original generations.

D.3 COMPARISON ON MORE BASELINES

In this section, we compare against more methods because of the page limit in our main paper, including ESD⁸ (Gandikota et al., 2023), RACE⁹ (Kim et al., 2024), Receler¹⁰ (Huang et al., 2024),

⁸<https://github.com/rohitgandikota/erasing>

⁹<https://github.com/chkimmmmm/R.A.C.E.>

¹⁰<https://github.com/jasper0314-huang/Receler>

Table 7: **Complete quantitative comparison of the few-concept erasure** in erasing artistic styles from Table 1 (right). The best results are highlighted in **bold**, and **grey columns** are indirect indicators for measuring erasure efficacy on target concepts or prior preservation on non-target concepts.

	<i>Van Gogh</i>		<i>Picasso</i>		<i>Monet</i>		<i>Paul Gauguin</i>		<i>Caravaggio</i>		MS-COCO	
	CS	FID	CS	FID	CS	FID	CS	FID	CS	FID	CS	FID
SD v1.4	28.75	-	27.98	-	28.91	-	29.80	-	26.27	-	26.53	-
Erase <i>Van Gogh</i>												
	CS ↓	FID ↑	CS ↑	FID ↓	CS ↑	FID ↓	CS ↑	FID ↓	CS ↑	FID ↓	CS ↑	FID ↓
ConAbl	28.16	129.57	27.07	77.01	28.44	63.80	29.49	63.20	26.15	79.25	26.46	18.36
MACE	26.66	169.60	27.39	69.92	28.84	60.88	29.39	56.18	26.19	69.04	26.50	23.15
RECE	26.39	171.70	27.58	60.57	28.83	61.09	29.58	47.07	26.21	72.85	26.52	23.54
UCE	28.10	133.87	27.70	43.02	28.92	40.49	29.62	32.62	26.23	61.72	26.54	19.63
ESD-X	27.04	200.05	26.50	111.07	28.14	90.35	29.45	106.70	25.70	107.85	26.10	33.19
ESD-U	26.24	205.06	26.28	153.10	27.79	105.78	29.59	164.83	26.14	124.41	26.35	38.08
RACE	23.03	233.25	25.54	127.28	26.44	94.49	27.78	106.43	25.08	114.94	25.92	41.52
Receler	21.53	245.40	24.88	134.35	23.61	143.17	25.02	194.58	24.52	133.94	25.95	37.00
Ours	26.29	131.02	27.96	35.86	28.94	16.85	29.71	24.94	26.24	39.75	26.55	20.36
Erase <i>Picasso</i>												
	CS ↑	FID ↓	CS ↓	FID ↑	CS ↑	FID ↓	CS ↑	FID ↓	CS ↑	FID ↓	CS ↑	FID ↓
ConAbl	28.66	60.44	26.97	131.45	28.72	36.23	29.68	65.23	26.20	79.12	26.43	20.02
MACE	28.68	59.58	26.48	137.09	28.73	37.02	29.71	46.35	26.23	66.20	26.47	22.86
RECE	28.71	51.09	26.66	126.40	28.87	25.39	29.69	46.08	26.22	75.61	26.48	23.03
UCE	28.72	37.58	26.99	102.21	28.92	16.72	29.71	32.48	26.22	59.27	26.50	20.33
ESD-X	28.58	104.48	26.07	178.18	28.32	62.79	29.31	96.70	25.84	100.54	26.15	34.12
ESD-U	28.69	109.39	26.47	156.35	28.64	67.69	29.64	95.39	26.04	105.76	26.35	35.78
RACE	28.12	112.29	24.84	185.78	27.88	72.79	28.91	93.19	25.81	110.23	25.77	42.01
Receler	25.92	199.56	23.10	243.28	26.92	94.89	26.51	208.01	25.34	135.35	25.88	37.20
Ours	28.76	19.18	26.22	117.71	28.88	19.87	29.75	24.73	26.24	43.63	26.51	19.98
Erase <i>Monet</i>												
	CS ↑	FID ↓	CS ↑	FID ↓	CS ↓	FID ↑	CS ↑	FID ↓	CS ↑	FID ↓	CS ↑	FID ↓
ConAbl	28.58	68.77	27.43	64.25	27.05	96.67	29.09	57.33	26.09	71.88	26.45	21.03
MACE	28.56	61.50	27.74	48.41	25.98	116.34	29.39	49.66	25.98	65.87	26.47	22.76
RECE	28.63	56.26	27.88	45.97	25.87	121.28	29.43	46.38	26.20	64.19	26.49	24.94
UCE	28.65	42.25	27.91	38.73	27.12	98.37	29.58	33.00	26.16	56.49	26.51	21.58
ESD-X	28.15	115.51	26.56	92.69	25.97	124.90	28.85	89.07	25.92	102.53	25.98	35.79
ESD-U	28.73	134.10	26.87	114.64	25.15	134.02	29.44	135.64	25.72	131.90	26.21	38.16
RACE	27.13	132.42	25.99	106.70	23.08	149.16	27.52	98.71	24.96	110.34	25.81	41.96
Receler	24.94	169.55	26.16	105.24	21.06	182.34	24.81	199.23	25.03	122.42	25.99	36.39
Ours	28.76	28.78	27.93	41.21	25.06	134.11	29.66	27.85	26.22	55.20	26.48	20.87

Table 8: **Quantitative comparison with SPM and SPM w/o FT in multi-concept erasure.** The best results are highlighted in **bold**. Our method is capable of erasing up to 100 celebrities at once with low Acc_e (%) and preserving other non-target celebrities with less appearance alteration with high Acc_r (%), resulting in the best overall erasure performance H_o (shaded in pink). **FAIL** indicates that the model collapses with noisy generations ($Acc_e = Acc_r = 0.00\%$).

	Erase 10 Celebrities			MS-COCO		Erase 50 Celebrities			MS-COCO		Erase 100 Celebrities			MS-COCO	
	Acc_e ↓	Acc_r ↑	H_o ↑	CS ↑	FID ↓	Acc_e ↓	Acc_r ↑	H_o ↑	CS ↑	FID ↓	Acc_e ↓	Acc_r ↑	H_o ↑	CS ↑	FID ↓
SD v1.4	91.99	89.66	14.70	26.53	-	93.08	89.66	12.85	26.53	-	90.18	89.66	17.70	26.53	-
SPM	0.00	51.79	68.24	26.42	48.44	0.00	0.00	FAIL	26.32	52.61	0.00	0.00	FAIL	25.15	63.20
SPM w/o FT	0.00	5.08	9.68	26.38	52.23	0.00	0.00	FAIL	16.22	170.68	0.00	0.00	FAIL	14.34	245.92
Ours	1.81	89.09	93.42	26.47	30.02	3.46	88.48	92.34	26.46	39.23	5.87	85.54	89.63	26.22	44.97

and SPM¹¹ (Lyu et al., 2024). While the first three methods are training-based, focusing solely on modifying model parameters, SPM not only fine-tunes the model weights using LoRA (Hu et al., 2021) but also intervenes in the image generation process through *Facilitated Transport*. Specifically, this module dynamically adjusts the LoRA scale based on the similarity between the sampling prompt and the target concept. In other words, if the prompt contains the target concept or is highly

¹¹<https://github.com/Con6924/SPM>

Table 9: **Evaluation of implicit concept erasure** in erasing *nudity* on four benchmarks. We report the Attack Success Rate (ASR) detected by NudeNet with a threshold of 0.6. ✓ and × indicate whether the method can defend against white-box attacks, respectively. The best and second-best results are marked in **bold** and underlined.

	I2P	MMA	Ring-A-Bell	UnlearnDiff	Time (s) ↓	MS-COCO		White-Box Attack
						CS	FID	
MACE (Lu et al., 2024a)	0.21	0.04	0.05	0.67	55 (×15)	24.06	52.78	✓
CPE (Lee et al., 2025b)	<u>0.07</u>	<u>0.01</u>	0.00	-	500 (×138)	26.32	48.23	×
AdvUnlearn (Zhang et al., 2024b)	0.04	0.00	0.00	0.21	15860 (×4400)	24.05	57.22	✓
UCE (Gandikota et al., 2024)	0.24	0.38	0.39	0.80	1.2 (×0.33)	26.24	38.60	✓
RECE (Gong et al., 2025)	0.14	0.20	0.18	0.65	1.5 (×0.41)	25.98	40.37	✓
RACE (Kim et al., 2024)	0.23	0.29	0.21	0.47	2910 (×800)	25.54	42.73	✓
Receler (Huang et al., 2024)	0.13	0.07	<u>0.01</u>	-	5560 (×1500)	25.93	40.29	×
Ours w/o AT	0.20	0.24	0.20	0.75	3.6 (×1)	26.29	37.82	✓
Ours w/ AT	0.10	<u>0.01</u>	0.00	<u>0.45</u>	4.5 (×1.25)	26.03	39.51	✓

Table 10: **Ablation study on the edited parameters.** Our scheme on only editing the value matrices achieves a superior balance between erasure efficacy (*e.g.*, target CS of 26.29) and prior preservation (*e.g.*, the lowest FIDs across all non-target concepts).

Ablation	Parameters		<i>Van Gogh</i>	<i>Picasso</i>	<i>Monet</i>	<i>Paul Gauguin</i>	<i>Caravaggio</i>	MS-COCO	
	Key	Value	CS ↓	FID ↓	FID ↓	FID ↓	FID ↓	CS ↑	FID ↓
1	✓	×	27.67	42.11	26.09	28.08	52.44	26.55	18.72
2	✓	✓	26.24	48.41	28.65	33.79	57.23	26.53	23.20
Ours	×	✓	26.29	35.86	16.85	24.94	39.75	26.55	20.36

relevant, this scale is set to a large value, whereas if there is little to no relevance, it is set close to 0, functioning similarly to a text filter. We argue that such a comparison with SPM is not fair since we only focus on modifying the model parameters, and therefore, we compare both the original SPM and SPM without *Facilitated Transport* (SPM w/o FT) for a fair comparison. In the latter version, the LoRA scale is set to 1 by default.

The quantitative comparative results are shown in Tables 6 and 7, where our method consistently achieves the best prior preservation compared to all compared baselines. Even equipped with *Facilitated Transport* (*i.e.*, SPM w/ FT), our method achieves the lowest non-target FID (*e.g.*, on *Pikachu* and *Hello Kitty*). This superiority amplifies as the number of target concepts increases as shown in Table 8. For example, with the number of target concepts increasing from 1 to 3, our FID in *Pikachu* rises from 16.81 to 21.40 (4.59 ↑), while SPM increases from 19.82 to 37.51 (17.69 ↑), where a similar pattern is observed in *Hello Kitty* (Our 4.48 ↑ *v.s.* SPM’s 15.68 ↑). Once removing the *Facilitated Transport* module, SPM w/o FT shows poorer prior preservation with rapidly increasing FIDs (highlighted in red in Table 6). More qualitative results are shown in Fig. 9.

D.4 ON IMPLICIT CONCEPT ERASURE

Evaluation setup. We evaluate the erasure efficacy on implicit concepts (*e.g.*, *nudity*), where the target concept does not explicitly appear in the text prompt. We conduct experiments on the Inappropriate Image Prompt (I2P) benchmark (Schramowski et al., 2023), which consists of various implicit inappropriate prompts involving violence, sexual content, and nudity. To evaluate adversarial robustness, we further introduce three adversarial attack benchmarks, including two black-box benchmarks (MMA (Yang et al., 2024b) and Ring-A-Bell (Tsai et al., 2023)) and one white-box benchmark (UnlearnDiff (Zhang et al., 2024c)). For concept erasure, we follow the setting in (Gong et al., 2025) to erase *nudity* → ‘ ’. During evaluation, we use NudeNet (Bedapudi, 2019) with a threshold of 0.6 to detect nude content and report the Attack Success Rate (ASR). Moreover, since the retain set only includes ‘ ’ in implicit concept erasure, we add an identity matrix \mathbf{I} with weight $\lambda = 0.5$ to the term $(\mathbf{C}_2^T \mathbf{P} \mathbf{M} \mathbf{C}_2)^{-1}$ in Eq. 12 to ensure invertibility.

Analysis and discussion. In addition to the aforementioned methods, we introduce more adversarial training-based methods for comparison, including CPE (Lee et al., 2025b), AdvUnlearn (Zhang et al., 2024b), RACE (Kim et al., 2024), and Receler (Huang et al., 2024). These methods enhance robustness against adversarial attacks by explicitly incorporating adversarial training objectives. We

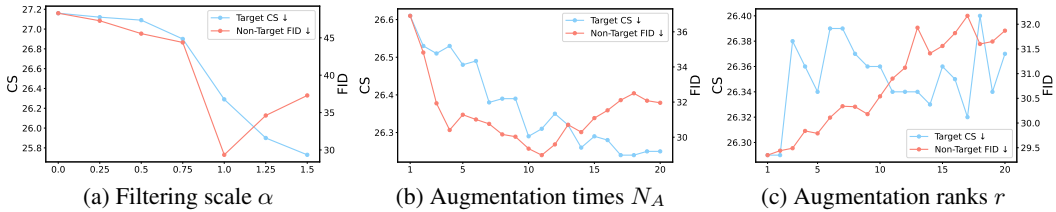


Figure 10: **Ablation study on hyperparameters.** We report target CS of erasing *Van Gogh* and non-target FID averaged over other four styles (*i.e.*, *Picasso*, *Monet*, *Paul Gauguin*, *Caravaggio*).

also adapt our method with adversarial training/editing (denoted as Ours w/ AT) following the setting in RECE (Gong et al., 2025) to provide a fair comparison. As shown in Table 9, we observe that adversarial training-based methods such as CPE and AdvUnlearn achieve strong erasure efficacy but incur extremely high computational costs. Editing-based approaches like UCE and RECE are more efficient yet less robust under both black-box and white-box attacks. Notably, CPE and Receler rely on additional modules for concept erasure, which makes them particularly vulnerable in the white-box setting since attackers can directly exploit these components to bypass erasure. In contrast, our method without adversarial training (Ours w/o AT) already offers a favorable balance between efficiency and prior preservation, and extending it with adversarial training/editing (Ours w/ AT) further improves robustness, reducing ASR across all benchmarks and lowering the white-box UnlearnDiff score from 0.75 to 0.45 while maintaining competitive runtime and prior knowledge preservation.

D.5 ABLATION STUDIES

Edited parameters. We compare the impact on editing different CA parameters in Table 10 and draw the following conclusions: (1) Only editing the key matrices cannot achieve effective erasure, with the target CS being 27.67 (*v.s.* the original CS of 28.75). This is because they mainly arrange the layout information of the generation and cannot effectively erase the semantics of the target concept. (2) Simultaneously editing both the key and value matrices can achieve effective erasure, but it will also excessively damage prior knowledge. (3) Only editing the value matrices achieves a superior balance between erasure efficacy and prior preservation. Compared to Ablation 2, the editing of key matrices leads to excessive erasure, which is unnecessary in concept erasure.

Filtering scale. We ablate the filtering threshold scale in the Influence-based Prior Filtering (IPF) module in Sec. 4.1 by scaling the impact scores μ with a factor α , which controls the strength of filtering influential priors. As shown in Fig. 10 (a), varying α directly affects the trade-off between erasure efficacy and prior preservation. When α is small (*i.e.*, close to 0), more weakly affected priors are included in the retain set, increasing its rank and overly shrinking the null space. This leads to worse erasure efficacy (higher CS) and poor preservation (higher FID). Conversely, a higher α yields better erasure performance due to fewer retain concepts, but still increases the FID because of non-comprehensive prior coverage. The best balance is observed at moderate thresholds (*e.g.*, $\alpha = 1$ in our setup), achieving both effective erasure and competitive prior preservation.

Augmentation times. We ablate the augmentation times N_A proposed in the Directed Prior Augmentation (DPA) module in Sec. 4.2, which controls the balance between semantic degradation and retain coverage along with the Influence-based Prior Filtering (IPF) module. It can be observed from Fig. 10 (b) that: (1) As N_A increases, the non-target FID exhibits a trend of first decreasing and then increasing. This suggests that when N_A is small (*i.e.*, $1 \rightarrow 10$), augmenting existing non-target concepts with semantically similar concepts facilitates a more comprehensive retain coverage, thereby improving prior preservation. However, when N_A exceeds a certain threshold (*i.e.*, $10 \rightarrow 20$), further augmentation of non-target concepts leads to narrowing the null-space derivation with semantic degradation, ultimately degrading prior preservation. (2) Target CS generally shows a declining trend, indicating that the proposed Prior Knowledge Refinement strategy not only improves prior preservation but also exerts a positive impact on erasure efficacy.

Augmentation ranks. Another hyperparameter to be ablated is the augmentation ranks r . From Eq. 7, we introduce the number of the smallest singular values, *i.e.*, augmentation ranks r in deriving $\mathbf{P}_{\min} = \mathbf{U}_{\min} \mathbf{U}_{\min}^T$ with $\mathbf{U}_{\min} = \mathbf{U}_{\mathbf{W}}[:, -r :]$. Mathematically, r represents the directions in which the DPA module can augment in the concept embedding space and constrains the rank of the

augmented embeddings to a maximum of r . As shown in Fig. 10 (c), as r increases, the non-target FID exhibits an overall upward trend, indicating that introducing more ranks does not benefit prior preservation, as it narrows the null space. At the same time, as shown in Table 3, such augmentation by DPA also remains necessary, as it enables more comprehensive coverage of non-target knowledge with semantically similar concepts, leading to improved prior preservation.

E LLM USAGE STATEMENT

We use large language models (LLMs) as an auxiliary tool during preparing this work. The LLM is employed to generate artistic style templates for the artistic style erasure task (see Appx. C.1) and to refine the clarity and readability of certain parts of the manuscript, such as polishing grammar, improving fluency, and standardizing terminology. In addition, LLMs are occasionally used to suggest alternative phrasings when writing sections like the introduction and related work, but the final narrative, arguments, and presentation choices are made solely by the authors. All methodological ideas, theoretical derivations, experiment designs, and analyses are developed independently by the authors without assistance from LLMs. We do not rely on LLMs for generating novel research ideas, conducting experiments, interpreting results, or writing technical content. The role of LLMs is purely supportive and limited to stylistic refinement and auxiliary text generation, and thus they are not regarded as scientific contributors to this paper.

F LIMITATION

Despite the promising results, SPEED is designed with linear null-space projections, which may not fully capture the nonlinear interactions between concepts in large diffusion models. In practice, this can lead to imperfect preservation when erasing highly entangled or stylistically subtle concepts. In addition, our evaluation mainly covers benchmarks with explicit or implicit concepts; the effectiveness on more abstract (*e.g.*, *freedom*), compositional (*e.g.*, *a blue cat*), or cultural (*e.g.*, *Día de los Muertos*) concepts remains less explored. Finally, although our method scales efficiently to 100 concepts, extending it to even larger-scale or continual erasure may require additional mechanisms.